

# 國立交通大學

機械工程學系

博士論文

質子交換膜燃料電池中陰極層汽液界面位置對  
性能之影響

Effects of the Gas-Liquid Interface Location in the Cathode  
Layer on the Performance of a PEM Fuel Cell

研究生：李純怡

指導教授：陳俊勳 教授

曲新生 教授

中華民國九十六年六月

質子交換膜燃料電池中陰極層汽液界面位置對  
性能之影響

Effects of the Gas-Liquid Interface Location in the Cathode  
Layer on the Performance of a PEM Fuel Cell

研究生：李純怡  
指導教授：陳俊勳、曲新生

Student : Chun-I Lee  
Advisor: Chiun-Hsun Chen  
Hsin-Sen Chu



Submitted to Department of Mechanical Engineering  
National Chiao Tung University  
in partial Fulfillment of the Requirements  
for the Degree of  
Doctor of Philosophy  
in  
Mechanical Engineering

June 2007

Hsinchu, Taiwan, Republic of China

中華民國九十六年六月

# 國立交通大學

## 論文口試委員會審定書

本校 機械工程 學系博士班 李純怡 君

所提論文(中文) 質子交換膜燃料電池中陰極層汽液界面位置對性能之影響

(英文) Effects of the Gas-Liquid Interface Location in the Cathode Layer on the Performance of a PEM Fuel Cell

合於博士資格水準、業經本委員會評審認可。

口試委員：陳朝光 洪哲文

顏維謀 楊文美

曲新生 陳俊逸

指導教授：陳俊逸 曲新生

系主任：陳俊逸 教授

中華民國九十六年六月二十九日

# 質子交換膜燃料電池中陰極層汽液界面位置對性能之影響

研究生：李純怡

指導教授：陳俊勳、曲新生

## 摘 要

本論文主要是探討三維、多物種、二相混合模式下之質子交換膜燃料電池中，其陰極增濕、陰極氣體擴散層的孔隙度、電池溫度以及增濕溫度的變化對燃料電池的傳輸現象及電池性能之影響。本研究中主要是利用沿著流道方向之汽液界面的位置來說明在這些操作條件下，液態水出現的位置對電池性能的影響。在研究過程中，首先先建立描述質子交換膜燃料電池內部各種傳輸及電化學現象之數學模式，其中以質量、動量、物種、能量及電流守恆方程式做為模式的主要方程式。在電化學反應中，主要的驅動力是利用活化過電位來作為陰極觸媒層中電子相電位與質子相電位的聯繫。而且當電池發生電化學反應時會產生熱能，其熱能的來源包括因電化學反應所造成之不可逆的熱及熵、因質子和電子傳輸所造成的焦耳熱以及因水的蒸發及凝結所產生的潛熱。因為本論文中考慮二相流動的傳輸，因此在此部分是利用  $M^2$  模式來說明其各物種之間的相互關係。

本研究探討的議題分為二個部份：第一部份是以等溫系統為主，即是不考慮能量方程式。主要是探討在陰極的流道及擴散層中，陰極的增濕情況以及陰極氣體擴散層的孔隙度改變時對汽液界面位置的影響。數值模擬的結果顯示當陰極的增濕程度逐漸增加以及電池的操作電壓逐漸降低時，汽液界面的位置會逐漸往流

道的入口方向移動。這是因為當陰極增濕度增加時，會有較多的液態水產生，而液態水會造成多孔隙材質中的孔穴被液態水佔據，造成燃料氣體傳輸的阻礙，因此電池性能降低。相同的，當電池電壓降低時，即是電流密度較大時，電化學反應較為快速，因此汽液界面的位置也會逐漸往流道的入口方向移動因而造成相同的情況。再者，當陰極的氣體擴散層孔隙度逐漸增加時，無論是水或是燃料氣體，皆較容易通過多孔隙材質，因此，當陰極氣體擴散層的孔隙度增加時，電池性能較佳。另外，沿著流道方向之氧氣分率、水分率以及液態水在陰極流道及擴散層中的分佈及變化也一併提出及探討。

第二部份主要是以非等溫系統為主，因為液態水的蒸發與凝結皆與操作溫度有著密切的關係，因此本部分考慮在不同的操作溫度時其對汽液界面位置的影響。操作溫度主要是分成電池溫度以及增濕溫度來探討。數值模擬的結果顯示當增濕溫度等於或大於電池溫度時，其汽液界面的位置會隨著電池溫度的降低而逐漸往流道的入口處移動，進而造成電池性能的降低。另外也分別探討在薄膜內的溫度分佈、在流道入口處陰極氣體擴散層內溫度以及液態水的分佈。並且清楚的指出燃料氣體在氣體擴散層中是利用擴散方式由流道往肋條的方向移動，反之，液態水在氣體擴散層中則是利用毛細作用力由肋條往流道出口處移動。

# **Effects of the Gas-Liquid Interface Location in the Cathode Layer on the Performance of a PEM Fuel Cell**

**Student: Chun-I Lee      Advisor: Chiun-Hsun Chen  
Hsin-Sen Chu**

## **ABSTRACT**

This dissertation presents a three-dimensional, multi-component, two-phase model to investigate the transport phenomena and performance of proton exchange membrane fuel cell as the liquid water forms under various cathode humidification conditions, gas diffusion layer porosities, cell temperatures, and humidification temperatures. In this study, the location of the gas-liquid interface along the channel direction is extracted to explain the effects of liquid water appearance that cause the cell performance change. A mathematical model, coupled with the electrochemical process, two-phase flows, species transfer, and heat transfer is developed at first. In the electrochemical reaction of the cathode catalyst layer, the solid phase potential and the electrolyte phase potential is connected by the activation overpotential. Furthermore, thermal energy release and transport is accompanied with the electrochemical reaction and is considered in modeling. The sources of thermal energy accounts for irreversible heat and entropic heat generated due to electrochemical reactions, Joule heating arising from protonic/electronic currents, and

latent heat of water condensation and/or evaporation. The multiphase mixture formulation ( $M^2$  model) is adopted as it is particularly suitable for two-phase flow modeling in PEM fuel cells.

Our quest to the effects of the liquid-water interface location involves the following two parts in the dissertation. First, we considered the isothermal system in the PEM fuel cell, namely the energy conservation equation is not included in it. The objective of this part is to investigate the effects of the location of the gas-liquid interface along the channel direction under various cathode humidification conditions and gas diffusion layer porosities in the conventional flow field. Numerical simulation results indicate that the gas-liquid interface location approaches to the gas flow channel inlet region and cell performance declines gradually as the relative humidity of the cathode is increased. This is because of liquid water may occupy the pores in the porous media, reducing the amount of fuel gas that can reach the cathode catalyst layer to cause the cell performance diminished. Meanwhile, when the cell operating voltage decreases and the current density gets larger, the electrochemical reaction becomes more quickly. Hence, the gas-liquid interface location also moves to the channel inlet region to cause the same consequence. Furthermore, as the gas diffusion layer porosity is increased, the transport of liquid water and fuel gas becomes easier and the cell performance is enhanced. To explain this phenomenon, the oxygen

fraction, the water fraction and the liquid water saturation field along the flow channel direction in the flow channel and the gas diffusion layer are presented.

The investigation of the location of the gas-liquid interface along the channel direction at various operating temperatures is conducted in the second part of the dissertation, owing to the consideration that the condensation and/or evaporation of the water is related with operating temperature. The effects of two model parameters, namely cell temperature ( $T_{cell}$ ) and humidification temperature ( $T_h$ ), on the gas-liquid interface location and cell performance are presented. Simulation results indicate that when the anode and cathode humidification temperatures are equal to or higher than the cell temperature, the gas-liquid interface location moves toward the flow channel inlet region and the cell performance decreases as the temperature is decreased. Additionally, the membrane temperature distribution and the distributions of the liquid water and temperature in the cross-section of the cathode gas diffusion layer in the inlet region are presented. Simulation results indicate that gas-phase fluid diffuses from the channel to the land and that the capillary-driven liquid water is transported in the opposite direction in the cathode gas diffusion layer.



## 誌 謝

在交大的求學過程中，首先先感謝恩師 曲新生及陳俊勳博士，恩師除了在學術上悉心的指導我之外，在待人處世方面更是值得我學習的榜樣。其次，感謝顏維謀、陳發林、宋齊有及鄭金祥博士在台大讀書會時給予我莫大的幫助，使我的博士論文能進行的更加順利。也很感謝口試委員陳朝光、洪哲文、楊文美及顏維謀諸位教授對於論文的建議及指導，使得本論文更加的嚴謹及完整。

此外，特別感謝木勝、輝忠及弘祥學長不厭其煩的幫助我修正論文及解決疑惑。也感謝研究室的學長及學弟們為我的生活帶來了許多歡樂的回憶。

最後，感謝我的家人—老爸、老媽、大哥、大嫂、二哥以及我的丈夫 Francis，在我求學的過程中，陪伴我經歷了許多挫折及挑戰，也給予我許多的幫助及鼓勵，使我能更堅定要完成學業的決心，僅以此論文獻給所有關心、愛護及幫助我的人，非常非常的感謝！

# TABLE OF CONTENTS

<b>ABSTRACT (in Chinese)</b> .....	<b>i</b>
<b>ABSTRACT (in English)</b> .....	<b>iii</b>
<b>LIST OF TABLES</b> .....	<b>ix</b>
<b>LIST OF FIGURES</b> .....	<b>x</b>
<b>NOMENCLATURE</b> .....	<b>xiv</b>
<b>CHAPTER 1 INTRODUCTION</b> .....	<b>1</b>
1.1 Background.....	<b>1</b>
1.1.1 Transport Phenomena in a PEMFCs.....	<b>2</b>
1.2 Literature Survey.....	<b>4</b>
1.3 Objectives.....	<b>14</b>
1.4 Outlines.....	<b>15</b>
<b>CHAPTER 2 MATHEMATICAL MODELING</b> .....	<b>20</b>
2.1 Model Description.....	<b>21</b>
2.2 Basic Assumptions.....	<b>22</b>
2.3 Governing Equations.....	<b>23</b>
2.4 Boundary Conditions.....	<b>30</b>
2.5 Numerical Procedures.....	<b>32</b>
2.5.1 Numerical Method.....	<b>32</b>
2.5.2 Calculation Procedure.....	<b>33</b>
2.5.3 Model Validation.....	<b>33</b>
<b>CHAPTER 3 EFFECTS OF CATHODE HUMIDIFICATION AND POROSITY OF THE GDL ON THE GAS-LIQUID INTERFACE LOCATION IN A PEM FUEL CELL</b> .....	<b>40</b>

3.1	Introduction.....	40
3.2	Effects of cathode humidification scheme .....	41
3.3	Effects of cell operating voltage.....	43
3.4	Three-dimensional species field.....	44
3.5	Two-phase mixture velocity field.....	47
3.6	Effects of the cathode gas diffusion layer porosity.....	47
3.7	Summary.....	51
<b>CHAPTER 4 EFFECTS OF TEMPERATURE ON THE LOCATION</b>		
<b>OF THE GAS-LIQUID INTERFACE IN A PEM FUEL</b>		
<b>CELL.....</b>		
		<b>67</b>
4.1	Introduction.....	67
4.2	Effects of temperatures scheme.....	68
4.3	Effects of cell temperatures scheme.....	69
4.4	Three-dimensional species field.....	71
4.5	Temperature field in the membrane.....	73
4.6	Summary.....	74
<b>CHAPTER 5 CONCLUSIONS AND FUTURE PERSPECTIVES .....</b>		
		<b>84</b>
5.1	Concluding Remarks.....	84
5.2	Future Perspectives.....	87
<b>REFERENCES.....</b>		
		<b>89</b>

# LIST OF TABLES

Table 2.1 Geometrical and operating parameters..... 35



## LIST OF FIGURES

Fig. 1.1.	Basic components of a single PEMFC.....	17
Fig. 1.2.	Operating principle of a single PEMFC.....	18
Fig. 1.3.	The dominant mechanisms of cell performance.....	19
Fig. 2.1.	Physical and computational domains considered in this study.....	36
Fig. 2.2.	Numerical flow diagram of the solution procedure.....	37
Fig. 2.3.	Comparison of predictions on the three different grid systems.....	38
Fig. 2.4.	Comparison of the predicted $I-V$ curve and the experimental data of Squadrito <i>et al.</i> [44].....	39
Fig. 3.1.	Effects of relative humidity of cathode on the location of the interface where liquid water begins to condense along the conventional flow channel at a cell operating voltage of 0.7 V. (a) $RH_{ca} = 20\sim 100\%$ and (b) $RH_{ca} = 20\sim 60\%$ .....	53
Fig. 3.2.	Effect of relative humidity of the cathode on cell performance with conventional flow fields. (a)I-V curves and (b) I-P curves.....	54
Fig. 3.3.	Effect of cell operating voltage on the location of the interface where liquid water begins to condense along the conventional flow channel at a relative humidity of the cathode of 80 %. (a) $V =$ $0.5\sim 0.9$ (b) $V = 0.8\sim 0.9$ .....	55
Fig. 3.4.	Oxygen fraction in the cathode gas channel and gas diffusion layer along the conventional flow channel at a cell voltage of 0.7 V and cathode relative humidity of 80%.....	56
Fig. 3.5.	Water fraction in the cathode gas channel and the gas diffusion layer along the conventional flow channel at a cell voltage of 0.7 V	

and cathode relative humidity of 80%.....	<b>57</b>
Fig. 3.6. Liquid water saturation field in the cathode gas channel and gas diffusion layer along the conventional flow channel at a cell voltage of 0.7 V and cathode relative humidity of 80 %.....	<b>58</b>
Fig. 3.7. Oxygen mass fraction contours at the gas diffusion layer at the cathode humidification of (a) 20% (b) 60% (c) 100% for cell voltage of 0.4 V.....	<b>59</b>
Fig. 3.8. Water mass fraction contours at the gas diffusion layer at the cathode humidification of (a) 20% (b) 60% (c) 100% for cell voltage of 0.4 V.....	<b>60</b>
Fig. 3.9. Liquid saturation contours at the gas diffusion layer at the cathode humidification of (a) 20% (b) 60% (c) 100% for cell voltage of 0.4 V.....	<b>61</b>
Fig. 3.10. Two-phase mixture velocity field in the gas diffusion layer and flow channel of the cathode at the cell voltage of 0.7 V and cathode relative humidity of 80%.....	<b>62</b>
Fig. 3.11. Effect of porosity of the gas diffusion layer on the location of the interface where liquid water begins to condense along the conventional flow channel at a cell voltage of 0.7 V and cathode relative humidity of 80%.....	<b>63</b>
Fig. 3.12. Effect of porosity of the gas diffusion layer on cell performance with conventional flow fields at cathode relative humidity of 80%. (a) <i>I-V</i> curves and (b) <i>I-P</i> curves.....	<b>64</b>
Fig. 3.13. Oxygen fraction at various porosities of the gas diffusion layer at an operating voltage of 0.7 V and cathode relative humidity of 80	

%.....	<b>65</b>
Fig. 3.14. Water fraction at various porosities of the gas diffusion layer at an operating voltage of 0.7 V and cathode relative humidity of 80 %.....	<b>66</b>
Fig. 4.1. Polarization curves at various cell temperatures with equal humidification temperature.....	<b>76</b>
Fig. 4.2. Effect of cell temperature on the location of the interface where liquid water begins to condense along the flow channel at a cell operating voltage of 0.7 V.....	<b>77</b>
Fig. 4.3. Polarization curves for various cell temperatures at (a) $T_h = 323$ K (b) $T_h = 343$ K.....	<b>78</b>
Fig. 4.4. Effects of cell temperature on the location of the interface where liquid water begins to condense along the flow channel at a cell operating voltage of 0.7 V and a humidification temperature of 343 K. (a) $Z = 0$ to 7.112 cm, (b) $Z = 0$ to 0.08 cm.....	<b>79</b>
Fig. 4.5. Liquid water saturation field in the cathode gas channel and diffusion layer along the flow channel at a cell voltage of 0.7 V and a humidification temperature of 343 K. (a) $T_{cell} = 323$ K, (b) $T_{cell} = 333$ K, (c) $T_{cell} = 343$ K.....	<b>80</b>
Fig. 4.6. Liquid water saturation distributions in a cross-section of the cathode gas diffusion layer in the inlet region at a cell voltage of 0.7 V and a humidification temperature of 343 K. (a) $T_{cell} = 323$ K, (b) $T_{cell} = 333$ K, (c) $T_{cell} = 343$ K.....	<b>81</b>
Fig. 4.7. Temperature distributions in a cross-section of the cathode gas diffusion layer in the inlet region at a cell voltage of 0.7 V and a	

humidification temperature of 343 K. (a)  $T_{cell} = 323$  K, (b)  $T_{cell} = 333$  K, (c)  $T_{cell} = 343$  K..... **82**

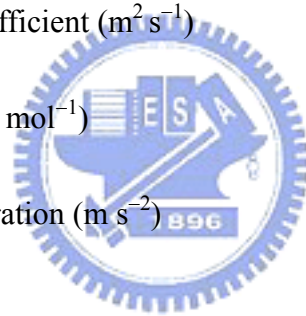
Fig. 4.8. Temperature contours in the membrane at a cell voltage of 0.7 V and a humidification temperature of 343 K. (a)  $T_{cell} = 323$  K, (b)  $T_{cell} = 333$  K, (c)  $T_{cell} = 343$  K..... **83**





# NOMENCLATURE

A	specific electrochemically active area
a	water activity
C	molar concentration ( $\text{mol m}^{-3}$ )
$C_F$	quadratic drag factor
$C_P$	constant-pressure heat capacity ( $\text{J kg}^{-1} \text{K}^{-1}$ )
$D^c$	capillary diffusion coefficient
$D_{ij}$	binary diffusion coefficient ( $\text{m}^2 \text{s}^{-1}$ )
F	Faraday constant ( $\text{C mol}^{-1}$ )
g	gravitational acceleration ( $\text{m s}^{-2}$ )
h	enthalpy ( $\text{J kg}^{-1}$ )
i	current density ( $\text{A m}^{-2}$ )
j	transfer current density ( $\text{A m}^{-3}$ )
K	permeability ( $\text{m}^2$ )
k	thermal conductivity ( $\text{W m}^{-1} \text{K}^{-1}$ )
M	molecular weight ( $\text{Kg mol}^{-1}$ )
$P^c$	capillary pressure
P	pressure (atm)



R universal gas constant ( $\text{J mol}^{-1} \text{K}^{-1}$ )

r rate constant

S source term

s liquid water saturation

T temperature (K)

T<sub>cell</sub> cell temperature (K)

T<sub>h</sub> humidification temperature (K)

$\bar{u}$  fluid velocity ( $\text{m s}^{-1}$ )

w mass fraction

x molar fraction



### **Greek**

$\alpha$  transfer coefficient

$\varepsilon$  porosity

$\phi$  phase potential (V)

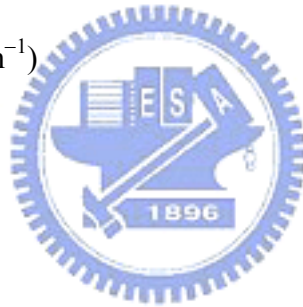
$\eta$  overpotential (V)

$\kappa$  proton conductivity ( $\text{S m}^{-1}$ )

$\lambda_k$  mobility of phase k

$\mu$  dynamic viscosity ( $\text{N s m}^{-2}$ )

$\nu$	kinematic viscosity ( $\text{m}^2 \text{s}^{-1}$ )
$\theta_c$	contact angle
$\rho$	density ( $\text{kg cm}^{-3}$ )
$\rho_k$	kinetic density ( $\text{kg m}^{-3}$ )
$\sigma$	electrical conductivity ( $\text{S m}^{-1}$ )
$\tau$	tortuosity of the porous medium
$\xi$	stoichiometric flow ratio
$\psi$	membrane water content
$\zeta$	surface tension ( $\text{N m}^{-1}$ )



### Subscripts

a	anode
c	cathode
con	condensation
e	electron
eva	evaporation
eff	effective value
g	gas phase
l	liquid phase

p      proton

sat      saturation value

w      water

### **Superscripts**

*ref*      reference value

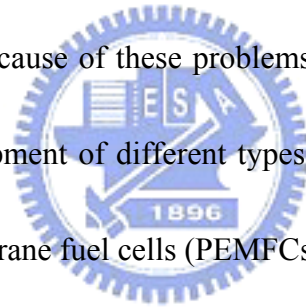


# CHAPTER 1

## INTRODUCTION

### *1.1 Background*

The depletion of fossil fuels and the degradation of the environment are key issues in modern society. There is an urgent need to substitute fossil fuels by renewable fuels and at the same time find new energy conversion methods that preserve the environment. Because of these problems, much effort has been devoted in recent years to the development of different types of fuel cells [1]. Among them, the polymer electrolyte membrane fuel cells (PEMFCs) have attracted much attention.



Proton exchange membrane fuel cell is a type of lower-temperature fuel cells and has been regarded as promising candidate of future power sources for both stationary and automotive applications. Especially for automotive applications, it is one of the most probable types of fuel cells which are able to replace conventional power conversion devices such as internal combustion engines because of its many distinctive features such as high energy efficiency, low noise, low emission, and especially low operating temperature (i.e., quick startup under environmental temperature). However, its performance must be improved and cost reduced before

this system becomes commercially available.

### **1.1.1 Transport Phenomena in a PEMFC**

Figure 1.1 shows the geometry of a single fuel cell, which consists of a membrane, two catalyst layers, two gas diffusion layers, two gas channels, and two collector plates. The major functions and characteristics of these components are: collector plates with flow channels are used for reactants and products transport, electron conduction and heat removal; gas diffusion layers are for reactant distributions, electron conduction, and liquid water removal; catalyst layers are used to promote electrochemical reactions where reactants are consumed, and products and heat are generated; and the membrane is used to conduct protons from the anode catalysts layer to the cathode catalyst layer. The electrochemical reaction occurring in the PEMFC is illustrated in Fig. 1.2. At the anode catalyst layer, hydrogen is consumed to produce protons and electrons, i.e.,



Electrons pass through an external circuit to the cathode thus providing electrical power, while the protons transport through the membrane to the cathode. At the cathode catalyst layer, oxygen combines with the protons and electrons to produce water, i.e.,



Although chemical reaction principles are rather simple, the transport processes inside a fuel cell are quite complex. First, the reactant species must be able to effectively transfer to different parts of the catalyst layers. Second, the electrical resistance to both protons and electrons must be low. And third, the product water and heat must be removed out of the fuel cell from the catalyst layers through the gas diffusion layers and other cell components. Further complications come from the dual effects of temperature and water.

A PEM fuel cell simultaneously involves electrochemical reactions, current distribution, hydrodynamics, multi-component transport, and heat transfer. Hence, a comprehensive mathematical model is needed to gain a fundamental understanding of the interacting electrochemical and transport phenomena. Nevertheless, polarization occurs during operation of PEM fuel cells and this influences dramatically both the performance and the commercialization of the technology. Accordingly, the development of a theoretical model of the PEM fuel cell, as well as corresponding analyses, are crucial to gain a good understanding of the effect of the operating conditions on the cell potential so that the polarization level can be well controlled.

Performance of a fuel cell is determined by several factors, including the geometry and morphology of transport components, and the operating conditions such as pressure, temperature and humidification of the reactant gases. And it is measured

by its current-voltage relation (i.e., the polarization curve), as shown in Fig. 1.3. At a particular current, the voltage drop is mainly caused by (i) overpotentials of electrochemical reactions (mainly on the cathode), (ii) the ohmic drop across the ionomeric membrane, and (iii) the mass transport limitations of reactants and products. At high current densities of special interest to vehicular applications, excessive water is produced within the cathode in the form of liquid, thus leading to a gas-liquid two-phase flow in the porous electrode. The ensuing two-phase transport of gaseous reactants to the reaction surface becomes a limiting mechanism for cell performance, particularly at high current densities.



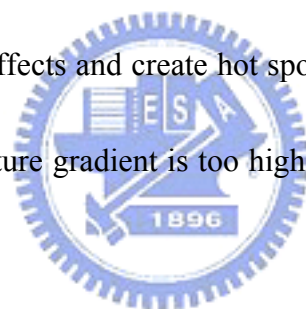
## ***1.2 Literature Survey***

Water and thermal management is essential for proper operation of PEM fuel cells. The polymer membrane in the PEM fuel cell must be in a highly hydrated state to facilitate proton transport. If there is not enough water, the membrane becomes dehydrated and its resistance to proton conduction increases sharply. On the other hand, if too much water is present, flooding may occur resulting in the pores of the gas diffuser filled by liquid water, which will block the transport of reactants to the reaction sites. In practice, humidification of anode fuels and/or cathode oxidants is often used to provide sufficient membrane hydration. Since water is produced in the



cathode catalyst layer and water also tends to migrate from the anode side to the cathode side under the electro-osmotic drag, it becomes a key issue to avoid flooding in the cathode in the design and operation of PEM fuel cells.

The influence of temperature on fuel cell operation has two important consequences. On one hand, higher temperature is favorable for electrochemical reactions. On the other hand, higher temperature also leads to a reduction in reactant partial pressure, cell open circuit voltage, and water activity, which results in an increase of membrane ionic resistance. In addition, non-uniform temperature distributions cause transient effects and create hot spots that may lead to cell failures. If the temperature or temperature gradient is too high, the fragile membrane could be damaged.



Modeling and computer simulation of PEM fuel cell began with the pioneering work of Bernardi and Verbrugge [2, 3] and Springer *et al.* [4, 5], whose models are essentially one-dimensional that provided good preliminary foundations for PEM fuel cell modeling. Bernardi and Verbrugge [2, 3] presented a one-dimensional model that included water transport. However, their model did not account for surface tension forces on the transport of the liquid phase. Also, the model was isothermal, and did not take into account energy interactions due to phase change. Springer *et al.* [4, 5] developed a one-dimensional isothermal model to predict the net water per proton

flux ratio across the membrane in PEM fuel cells. However, the one-dimensional model cannot simulate the decrease of reactants and the accumulation of products in the flow direction. In the pseudo two-dimensional model proposed by Fuller and Newman [6] and Nguyen and White [7], the effects of reactant consumption along the flow channels were considered. Nguyen and White [7] developed a two-dimensional PEM fuel cell model with one-dimensional heat transport in the flow direction. The model considered phase change of water in the flow channel as the only heat source. Both of these models assumed a well-mixed concentration in the flow channel, diffusion was the only mechanism for oxygen transport, the interaction of the flow with the species field in the channel and gas diffusion layer was not included. Subsequently, Yi and Nguyen [8] modified the previous models to include both the liquid and gas phase along the flow channel of both anode and cathode sides of PEM fuel cell. The results indicated that anode humidification improved the conductivity of the membrane, and that the cell performance is enhanced by the injection of liquid water and the increase in humidification temperature. Gurau and Liu [9] presented a two-dimensional model by coupling the flow and transport governing equations in the flow channel and the gas diffusion layer, but the density change due to species consumption appeared to be neglected. Yi and Nguyen [10] developed a two-dimensional hydrodynamics and multi-component transport in an interdigitated

cathode. However, this model is valid only in the absence of liquid water, and it does not account for water condensation and evaporation phase change within porous electrodes.

Several models have been developed to demonstrate the influence of liquid water on water management. Wang *et al.* [11] first studied two-phase flow and liquid water transport on the cathode side of a PEM fuel cell based on the multiphase mixture model ( $M^2$  model) originally developed by Wang and Cheng [12]. The model encompassed both single- and two-phase regimes corresponding to low and high current densities and was capable of predicting the transition between the two regimes. The half cell domain including the gas channel, gas diffusion, and catalyst layer on the cathode side of a PEM fuel cell was considered in the article. Later, this model was further developed to include a complete cell by You and Liu [13]. They presented a two-dimensional two-phase mixture model to analyze flow and transport in the cathode of the PEM fuel cell, and to predict phase change and water/oxygen distribution in both the flow channels and the porous diffusion layer. Also, such a two-phase model provides actual characteristics of the flow and the transport of reaction gas for thermal/water management design in the future. In Refs. [14, 15], Mazumder and cole developed a three-dimensional model to predict the effect of the formation of liquid water on the performance of the PEM fuel cell. In Ref. [14], the

polarization behavior was overestimated, based on the assumption that no liquid water was formed. In contrast, when liquid water was present, the condensation and/or evaporation of water via equilibrium phase transformation proceeded as described in Ref. [15]. They presented a numerical study, also based on the  $M^2$  model of Wang and Cheng. Since water condensation can obstruct pores and reduce cell performance, the polarization behaviors of PEM fuel cell must be accurately predicted to investigate such a situation. Pasaogullari and Wang [16] developed a model to explore the two-phase flow physics in the cathode gas diffusion layer. The simulations revealed that flooding of the porous cathode reduced the rate of oxygen transport to the cathode catalyst layer. Furthermore, they indicated that the humidification level and the flow rate of reactant streams are key parameters controlling PEM fuel cell performance and two-phase flow and transport characteristics. He *et al.* [17] proposed a two-dimensional, two-phase, multi-component transport model for PEM fuel cell with interdigitated flow field, in which they included capillary transport of liquid water in a completely wetted gas diffusion layer. They studied the effects of various electrode and flow field design parameters on the performance of the cathode of a PEM fuel cell. Natarajan and Nguyen [18] published a two-dimensional model that considered the dimension normal to the reactive surface and the electrode width. In this work, gas transport was modeled by Stefan–Maxwell multi-component diffusion equations,

while Darcy's law was adapted to model liquid water transport in unsaturated porous gas diffusion layers. Here the effect of liquid water accumulation in the diffusion layer was accounted for in terms of gas transport restrictions and reactive surface coverage. Meng and Wang [19] improved their three-dimensional computational fluid dynamics model based on recent visualization experiments, more accurately investigated the two-phase behavior under different gas utilizations. Their model was applied to successfully predict liquid water flooding dynamics although the energy transport was ignored. Zhang *et al.* [20] experimentally and theoretically studied the liquid water transport and removal from the gas diffusion layer and gas channel of the PEM fuel cells. In situ observations of the distribution of liquid water on the gas diffusion layer surface and inside the gas channel were made. They characterized the formation and emergence of liquid water from the gas diffusion layer surface and identified two modes of liquid water removal from the gas diffusion layer surface.

Thermal management in a PEM fuel cell is inherently coupled with water management, and the two factors combine to ensure high performance and durability of a PEM fuel cell. It is thus of paramount importance to understand the thermal behavior under various design and operating conditions and furthermore develop a capability to accurately predict the temperature distribution in PEM fuel cells. Rowe and Li [21] developed a one-dimensional model in the through-membrane direction.

Including entropic, irreversible, and phase change heats, they further took account of Joule heating in the membrane and anode/cathode catalyst layers. This work predicted the temperature variation in the through-membrane direction under the various current densities and electrode thermal conductivities. A major drawback of this model is the fact that the cathode catalyst layer is assumed to be fully hydrated and the membrane water content is linearly interpolated, indicating inapplicability of the model in low humidity operation. Baschuk and Li [22] developed a mathematical model with variable degrees of water flooding in the PEMFC. Physical and electrochemical processes occurring in the membrane electrolyte, the cathode catalyst layer, the electrode backing layer and the flow channel were considered. Compared with experimental results, they found that when air was used as the cathode fuel, the flooding phenomena are similar at different operating conditions of the pressures and temperatures. When cell pressure is increased significantly, the water flooding in the electrode becomes serious and leads to a noticeable reduction in the power output. To examine the effects of temperature and gas pressure gradients on fuel cell performance and water management, a one-dimensional, non-isothermal model was proposed by Djilali and Lu [23]. It was found that the temperature distribution in the PEM fuel cell is affected by the water phase change in the electrode. Simpalee and Dutta [24] formulated a comprehensive three-dimensional model to predict

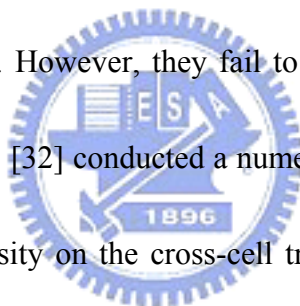
temperature distribution inside a straight channel PEMFC and to study the effect of heat produced by the electrochemical reactions on fuel cell performance. Source terms for transport equations, heat generation, and a phase change model were presented to facilitate their modeling work. They treat the liquid water as a component of the gas mixture, transported by convection by gas pressure and density gradients. The results showed that the temperature profiles depend on heat generation produced by electrochemical reactions and phase change of water inside the fuel cell. Further, the cell performance does not merely influenced by the inlet humidity condition, cell voltage, and membrane thickness but also by the temperature rise inside fuel cells. Natarajan and Nguyen [25] developed a pseudo three-dimensional model by extending a two-dimensional isothermal model for conventional flow fields. Their results indicated that water removal by evaporation increases with higher temperature and higher stoichiometric flow rates, which results in better cell performance. However, if the water produced by the electrochemical reaction could not effectively removed from the cathode side, then flooding of the electrode will occur, reducing access of the reactants to the catalyst layer. Yang *et al.* [26] reported the mechanics of the liquid water transport, starting from emergence on the gas diffusion layer surface, droplets grow and move toward the main stream flow in gas channels. Furthermore, the oversaturated water vapor causes more liquid film formation on hydrophilic

channel walls and the subsequent channel clogging affects cell performance. Liu *et al.* [27] experimentally studied the two-phase flow of reactants and products as well as water flooding situation in the gas flow channel of a cathode in a PEM fuel cell with three flow fields. Their study addressed the effects of flow field, cell temperature, cathode gas flow rate, operation time on water build-up, and cell performance. The results indicated that liquid water forms in columns that accumulate in the cathode flow channels and clogs the porous media, limiting mass transfer, resulting in degraded cell performance. Further, the amount of water in flow channels at high temperature is much less than that at low temperature. Ju *et al.* [28] presented the first work that systematically derived mathematical model of the energy equation from thermodynamics. The thermal model is further coupled with the electrochemical and mass transport to deal with the heat and water management in PEM fuel cell. Later, Wang and Wang [29] expanded the  $M^2$  model to investigate the interaction between the two-phase flow and thermal transport by non-isothermal effect. The results reveal that the vapor-phase diffusion enhances water removal and provides a new mechanism for heat removal through a phase change process. This new heat removal mechanism is similar to the heat pipe effect.

Much effort has been expended in recent years upon development of numerical models with increasingly less restrictive assumptions and more physical



complexities. Current development in PEM fuel cell modeling is in the direction of applying computational fluid dynamics (CFD) to solve the complete set of transport equations governing mass, momentum, species, energy, and charge conservation. Dutta *et al.* [30, 31] developed a complete three-dimensional simulation of PEM fuel cell using Fluent, a commercial CFD package. Their modeled domain covered the entire fuel cell sandwich employing conventional gas distributors on both the anode and the cathode sides. This model treats the MEA as an interface without thickness and ignores the membrane water storage capability; thus this model cannot be used to simulate transient phenomena. However, they fail to account for liquid water in the gas diffusion layers. Yan *et al.* [32] conducted a numerical study of the effects of fuel channel width and GDL porosity on the cross-cell transport of reactant gas and the performance of a PEM fuel cell. They [33, 34] subsequently presented a two-dimensional numerical model to carry out the reactant gas transport phenomena and cell performance with baffle effects in the flow channel of bipolar plate. Effects of the baffle width are explored. Additionally, the effects of liquid water formation on the reactant gas transport are taken into account in the modeling and examined in the analysis. A comprehensive non-isothermal, three-dimensional computational model of a PEM fuel cell has been developed by Berning *et al.* [35, 36]. The model incorporates a complete cell with both the MEA and the gas distribution flow



channels. With the exception of phase change, the model accounts for all major transport phenomena. The model is implemented in a CFD code, and simulations are presented with an emphasis on the physical insight and fundamental understanding afforded by the detailed three-dimensional distributions of reactant concentrations, current densities, temperatures and water fluxes. Um and Wang [37] presented a computational fuel cell dynamics model to elucidate three-dimensional interactions between mass transport and electrochemical kinetics in polymer electrolyte fuel cells with straight and interdigitated flow fields, respectively. The model results indicate that forced convection induced by the interdigitated flow field substantially improves mass transport of oxygen to, and water removal from, the catalyst layer, thus leading to a higher mass-transport-limiting current density as compared to that of the straight flow field. Chiang and Chu [38, 39] presented a three-dimensional, multi-species and two-phase model by CFD code to investigate the effects of temperatures, humidification levels, channel aspect ratio and gas diffusion layer thickness on the cell performance.

### ***1.3 Objectives***

The above literature review clearly indicates that water and thermal management are critical issues in the PEM fuel cell investigations. Because of the

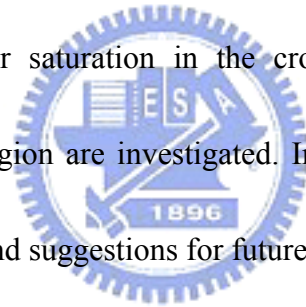
formation of liquid water depends on the saturation vapor pressure, which is a strong function of temperature. Therefore, the temperature factor is inevitable in water management investigation because the phase change of water such as condensation and/or evaporation closely relates to the corresponding saturation pressure. However, the discussions of the effect of gas-liquid interface location on the cell performance and transport process are rarely seemed. Therefore, this study investigates the formation and influence of the gas-liquid interface location along the flow channel direction at various operation conditions with a three-dimensional, multi-component, and two-phase model of a PEM fuel cell.



#### **1.4 Outlines**

The scope of this dissertation is mainly focused on four parts. Chapter 2 introduces the homogeneous model of the multiphase mixture formulation ( $M^2$  model) development as it is particularly suitable for two-phase flow modeling and applying computational fluid dynamics (CFD) to solve the complete set of transport equations governing mass, momentum, species, energy, and charge conservation in a PEM fuel cell. Furthermore, the proposed model incorporates the basic assumptions is also presented. Chapter 3 investigates the effects of cathode humidification and gas diffusion layer porosity on the location of the interface when the liquid water began to

condense along the flow channel of a PEM fuel cell; its contribution to the cell performance is also discussed. Additionally, the resulting oxygen and water fraction distributions and liquid water saturation fields at fixed cathode humidity are obtained to validate the simulation results. Chapter 4 reports the formation and influence of the gas-liquid interface location along the flow channel direction at various cell temperatures and humidification temperatures with a non-isothermal, three-dimensional, multi-component, and two-phase model of a PEM fuel cell. The temperature distribution in the cell domain membrane and the distributions of temperature and liquid water saturation in the cross-section of the cathode gas diffusion layer in the inlet region are investigated. In Chapter 5, the conclusions of this investigation are drawn and suggestions for future study are proposed.



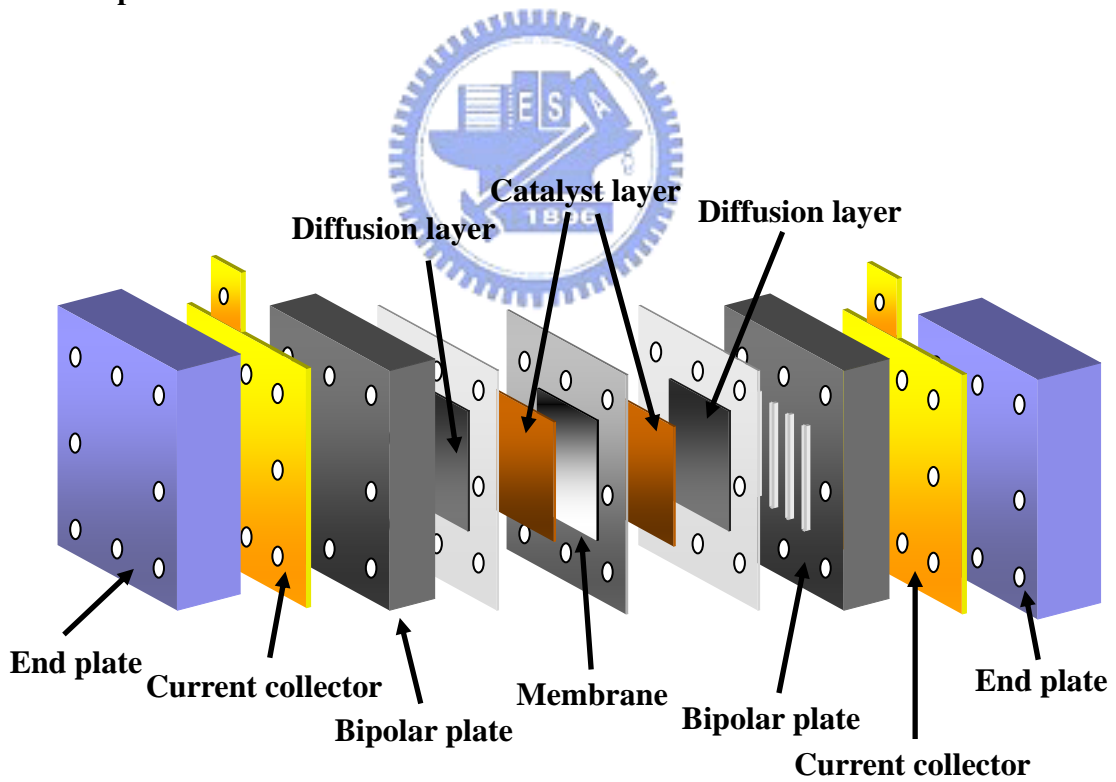
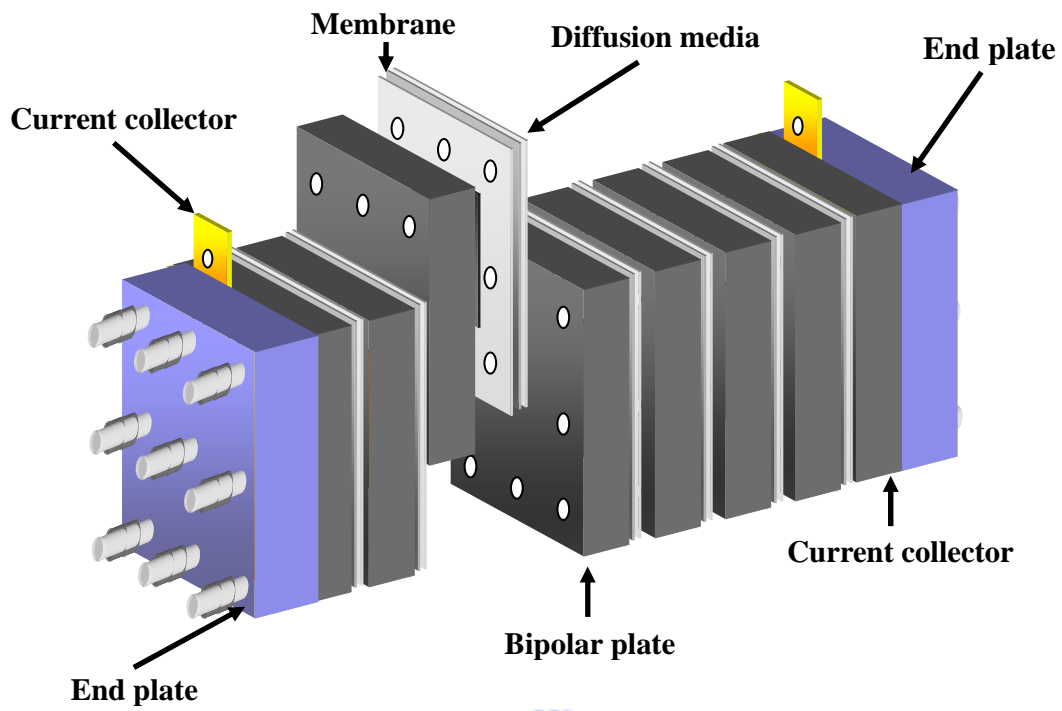


Figure 1.1 Basic components of a single PEMFC

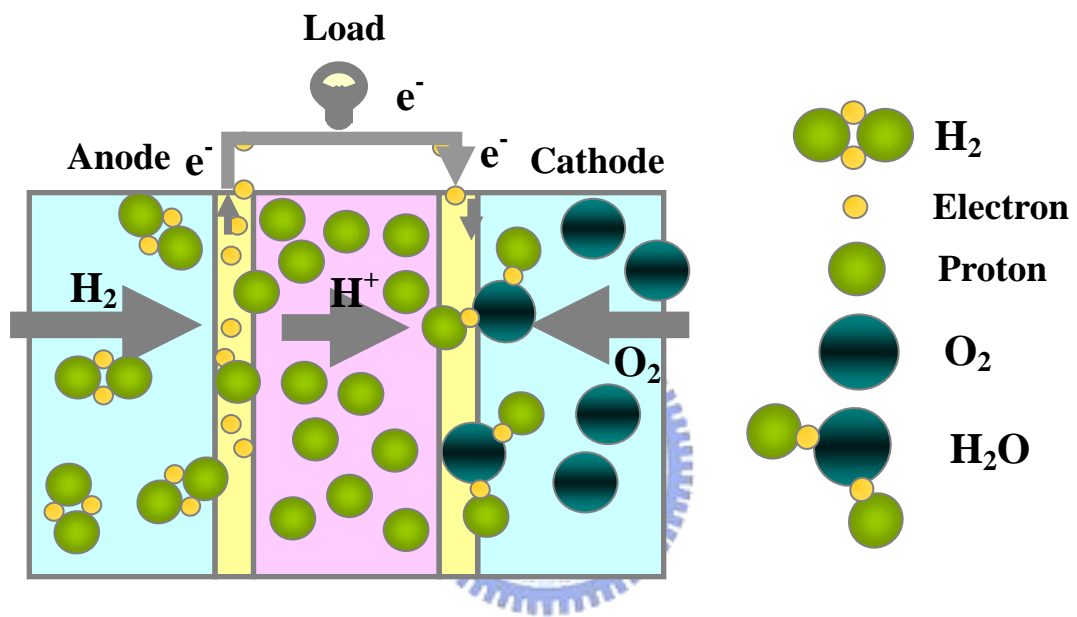


Figure 1.2 Operating principle of a single PEMFC

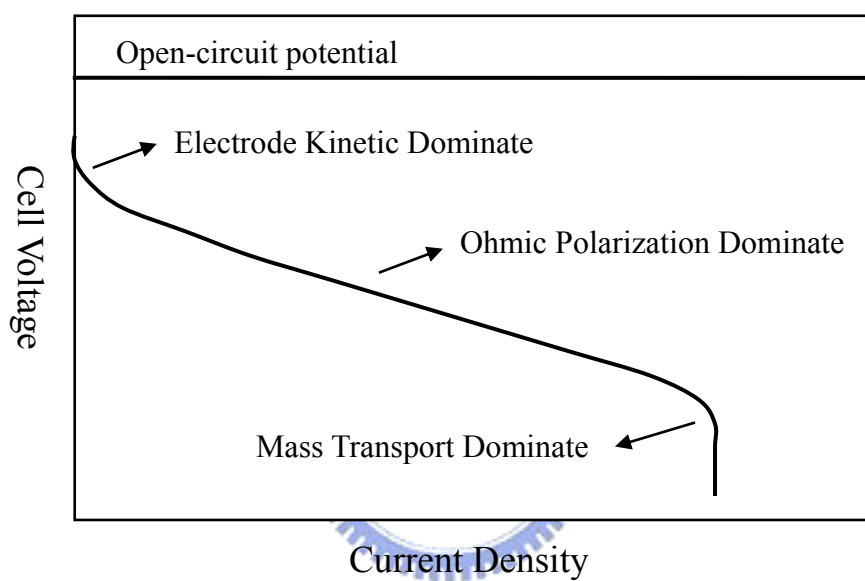


Figure 1.3 The dominant mechanisms of cell performance

## CHAPTER 2

### MATHEMATICAL MODELING

Traditionally, macroscopic problems of two-phase flow and transport in porous media have been modeled using a two-fluid approach. However, this approach results in a large number of primary variables for each phase, and highly nonlinear equations. Therefore, exact solutions of two-phase problems with two-fluid models are limited to a very limited number of problems with many simplifying assumptions. Furthermore, the two-fluid models require explicitly tracking the irregular and moving interface between two phases, increasing the numerical complexity of the problem. Particularly in PEM fuel cells, the gas-liquid interfaces, *i.e.*, the condensation and evaporation fronts, are expected as well as the coexistence of single- and two-phase regions. Therefore, a convenient model capable of describing both single- and two-phase regions without a need to track the irregular, a priori unknown interface is required. For these reasons, the multiphase mixture ( $M^2$ ) formulation of Wang and Cheng [12] is particularly suitable for two-phase PEM fuel cell modeling. The multiphase mixture model is a mathematical reformulation of the classical two-phase model that views the multiphase system as a chemical mixture. With this approach,



the multiphase flow is then described in terms of a mass-averaged mixture velocity and diffusive flux, representing the difference between the mixture velocity and individual phase velocity. One major advantage of the  $M^2$  model over the classical two-fluid models is that it eliminates the need for tracking phase interfaces, thus simplifying the numerical complexity of two-phase flow and transport modeling. Another salient feature of the  $M^2$  model for PEM fuel cell is that all model equations are valid in all three types of regions possible in a PEM fuel cell: single-phase (gas), liquid-gas (two-phase), and single-phase (liquid). Finally, the  $M^2$  model is mathematically equivalent to two-fluid models without invoking any additional approximations. These aforementioned advantages render the  $M^2$  model to be a suitable and widely adopted two-phase flow and transport modeling framework for PEM fuel cells [11, 13, 15].

In this chapter, a three-dimensional, two-phase, multi-component model of a PEM fuel cell is presented and the present analytical study focus on two-phase transport taking place in the cathode due to the production of water in the cathode catalyst layer.

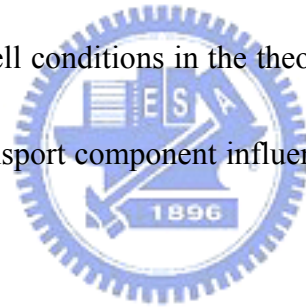
## ***2.1 Model Description***

The physical model employed in this study consists of nine parts, namely

bipolar plates, gas flow channels, gas diffusion layers, and catalyst layers on both the anode and cathode sides, and a polymer membrane that is sandwiched between them, as illustrated in Fig. 2.1. Symmetry is assumed, and a single straight flow channel is therefore considered herein.

## 2.2 *Basic Assumption*

Utilizing the homogeneous model of  $M^2$  formulation for two-phase transport, the proposed model incorporates the following assumptions. These basic assumptions are made to simplify actual cell conditions in the theoretical model and thus facilitate the modeling approach of transport component influence on transport phenomena and cell performance.



- The gaseous phase of the working fluid behaves as an ideal gas and the liquid water is incompressible;
- The Reynolds number of the fluid is below 100 because the velocity of the mixture is low, and the flow is considered to be laminar;
- The properties of the porous medium are isotropic and homogeneous.
- The system operates in a steady state;
- The thermal conductivities of the cell components are constant.

### 2.3 Governing Equations

The three-dimensional, multi-component, and two-phase model of a PEM fuel cell includes five nonlinear coupled conservation equations of mass, momentum, energy, species, and charge, which are described as follows.

#### Mass conservation equation

Since the gaseous and liquid water are present simultaneously in the control volume, the conservation equation of mass for a multiphase mixture is:

$$\nabla \cdot (\varepsilon_{eff} \rho \bar{u}) = 0 \quad (2.1)$$

where  $\rho$  represents the density of the mixture and is defined as the volume-weighted average of the phase mass concentration in two-phase flow [11]. When the liquid water is present, the effective porosity is given by  $\varepsilon_{eff} = \varepsilon(1 - s)$ .

#### Momentum conservation equation

The general form of the Navier–Stokes equation is used with source terms that describe the drag forces in the porous medium. The equation is:

$$\nabla \cdot (\rho \varepsilon_{eff} \bar{u} \bar{u}) = -\varepsilon_{eff} \nabla P + \nabla \cdot (\varepsilon_{eff} \mu_{eff} \nabla \bar{u}) + \varepsilon_{eff} \rho_k \mathbf{g} + S_m \quad (2.2)$$

where  $\mu_{eff}$  is the effective viscosity of the mixture,  $\rho_k$  is the kinetic density, and  $S_m$  is the sum of the Darcy and the Forchheimer drag forces,

$$S_m = -(\vec{F}_{Darcy} + \vec{F}_{Forch}) \quad (2.3)$$

which are given by:

$$\text{Darcy drag force} = \vec{F}_{Darcy} = \frac{\varepsilon_{eff}^2 \mu_{eff} \vec{u}}{K} \quad (2.4)$$

$$\text{Forchheimer drag force} = \vec{F}_{Forch} = \frac{\varepsilon_{eff}^3 C_F \rho}{\sqrt{K}} |\vec{u}| \vec{u} \quad (2.5)$$

The parameters  $C_F$  and  $K$  represent the quadratic drag factor and the permeability.

### Species conservation equation

The species conservation equation for the gas mixture is

$$\nabla \cdot (\varepsilon_{eff} \vec{u} C_k) = \nabla \cdot (D_{k,eff} \nabla C_k) + S_c \quad (2.6)$$

where  $k$  represents the chemical species, including hydrogen, oxygen, nitrogen, and water.  $D_{k,eff} = D_k \varepsilon^\tau$  represents the effective diffusion coefficient of the  $k$ -th component of the fuel reactant [17]. The exponent  $\tau$  on the porosity  $\varepsilon$  is the tortuosity of the porous medium. The source term  $S_c$  defines the production or consumption of the  $k$ -th species in the gas phase and is given by:

$$H_2 : -\frac{1}{2FC_a} j_a \quad (2.7)$$

$$O_2 : -\frac{1}{4FC_c} j_c \quad (2.8)$$

$$H_2O : \frac{1}{2FC_c} j_c \quad (2.9)$$

The terms  $j_a$  and  $j_c$  are defined as,

$$j_a = A j_0^{ref} \left( \frac{C_{H_2}}{C_{H_2}^{ref}} \right) \left[ e^{(a_a F/RT)\eta} - \frac{1}{e^{(a_c F/RT)\eta}} \right] \quad (2.10)$$

$$j_c = A j_0^{ref} \left( \frac{C_{O_2}}{C_{O_2}^{ref}} \right) \left[ e^{(\alpha_a F/RT)\eta} - \frac{1}{e^{(\alpha_c F/RT)\eta}} \right] \quad (2.11)$$

The above conservation equations of mass, momentum, and species are derived on the basis of the M<sup>2</sup> model. The constitutive relationships of mixture parameter and variables are all dependent on the liquid saturation, defined as the ratio of the liquid volume to the pore volume:

$$s = \frac{V_l}{V_{pore}} \quad (2.12)$$

$$\text{Density: } \rho = \rho_l s + \rho_g (1 - s) \quad (2.13)$$

$$\text{Concentration: } \rho C = \rho_l C_l s + \rho_g C_g (1 - s) \quad (2.14)$$

$$\text{Effective porosity: } \varepsilon_{eff} = \varepsilon (1 - s) \quad (2.15)$$

$$\text{Kinetic density: } \rho_k = \rho_l \lambda_l(s) + \rho_g \lambda_g(s) \quad (2.16)$$

$$\text{Effective viscosity: } \mu_{eff} = \frac{\rho_l s + \rho_g (1 - s)}{(k_{rl}/\nu_l) + (k_{rg}/\nu_g)} \quad (2.17)$$

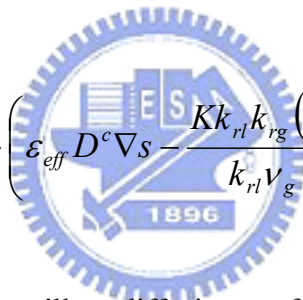
$$\text{Relative permeability: } \begin{cases} k_{rl} = s^3 & \text{liquid phase} \\ k_{rg} = (1 - s)^3 & \text{gas phase} \end{cases} \quad (2.18)$$

$$\text{Relative mobility: } \begin{cases} \lambda_l(s) = \frac{k_{rl}/\nu_l}{k_{rl}/\nu_l + k_{rg}/\nu_g} & \text{liquid phase} \\ \lambda_g(s) = 1 - \lambda_l(s) & \text{gas phase} \end{cases} \quad (2.19)$$

### Liquid water transport

During the operation of a fuel cell, liquid water forms if the partial pressure of

water vapor exceeds the saturation vapor pressure. The liquid water thus formed may occupy the pores and thereby prevent the diffusion of fuel, causing mass transport overpotential in the porous medium. Hence, the effect of liquid water is taken into account. Additionally, capillary forces dominate the transport of liquid water on the hydrophilic surfaces because the pores in the porous medium are extremely small. Therefore, the generalized Richards equation, developed by Wang and Beckermann [12, 40] to elucidate the two-phase flow transport in capillary porous media, is applied:



$$\nabla \cdot (\varepsilon_{eff} \rho \bar{u} \lambda_l(s)) = \nabla \cdot \left( \varepsilon_{eff} D^c \nabla s - \frac{K k_{rl} k_{rg} (\rho_l - \rho_g) \mathbf{g}}{k_{rl} v_g + k_{rg} v_l} \right) + S_l \quad (2.20)$$

where  $D^c$  and  $P^c$  represent the capillary diffusion coefficient and the capillary pressure, respectively:

$$D^c = - \frac{K k_{rl} k_{rg} (dP^c / ds)}{k_{rl} v_g + k_{rg} v_l} \quad (2.21)$$

$$P^c = \zeta \cos \theta_c \left( \frac{\varepsilon_{eff}}{K} \right)^{1/2} J(s) \quad (2.22)$$

and where  $J(s)$  is the Leverett function, which takes the following form [41, 42]:

$$J(s) = \begin{cases} 1.417(1-s) - 2.12(1-s)^2 + 1.263(1-s)^3 & \theta_c < 90^\circ \\ 1.417s - 2.12s^2 + 1.263s^3 & \theta_c > 90^\circ \end{cases} \quad (2.23)$$

In Eq. (2.22), the contact angle,  $\theta_c$ , of the gas diffusion layer is dependent upon the hydrophilic ( $0^\circ < \theta_c < 90^\circ$ ) or hydrophobic ( $90^\circ < \theta_c < 180^\circ$ ) nature of this layer, and varies with the Teflon content. We assume here that the gas diffusion layer is a hydrophilic medium. Further, the surface tension,  $\zeta$ , for the liquid water-air system is taken as 0.0625 N/m [41].

The source term  $S_l$  is a simplified switch function between condensation and/or evaporation of liquid water under these non-equilibrium conditions [15]. When the partial pressure of water vapor exceeds the saturation pressure of water, liquid water may form and occupy the pores in the porous medium. Conversely, the liquid water will evaporate if the partial pressure of water vapor is less than the saturation pressure of water:

$$S_l = \begin{cases} M_l r_{con} \frac{\varepsilon_{eff} x_w}{RT} (x_w P - P_{sat}), & \text{if } x_w P > P_{sat} \\ r_{eva} \varepsilon_{eff} s \rho_l (x_w P - P_{H_2O}), & \text{if } x_w P < P_{sat} \end{cases} \quad (2.24)$$

where  $r_{con}$  and  $r_{eva}$  are the condensation and evaporation rate constants, respectively;  $x_w$  is the molar fraction of water vapor, and  $P_{sat}$  is the saturation pressure of water, which varies with the temperature [4].

$$\log_{10} P_{sat} = -2.1794 + 0.02953T - 9.1837 \times 10^{-5} T^2 + 1.4454 \times 10^{-7} T^3 \quad (2.25)$$

### Energy conservation equation

The heat generation sources in a PEM fuel cell account for the irreversible heat and entropic heat that is generated by electrochemical reactions, Joule heating that arises from proton/electronic resistance, and the latent heat of water condensation and/or evaporation. A generalized energy conservation equation is:

$$\nabla \cdot (\varepsilon_{eff} \rho C_p \bar{u} T) = \nabla \cdot \left( k_{eff} \nabla T + \sum_{i=1}^n \sum_{j=1}^{n-1} \rho D_{ij} \nabla w_j h_i \right) - S_\eta + \frac{|i \cdot i|}{\sigma} + S_T \quad (2.26)$$

where  $k_{eff}$  represents the effective thermal conductivity. On the right-hand side of the equation, the first two terms represent the conduction energy and the reactant enthalpy flux; the third and fourth terms represent electrical-related thermal effects, and the last term is a source term, associated with the phase change.

### Charge conservation equation

In a fuel cell, the potential gradient effect causes electrons and protons to move along individual paths. Solid phase potential controls the movement of electrons. Electron transport generally occurs only in the bipolar plates, the diffusion layers, and the catalyst layers. However, ionomer phase potential controls the motion of protons, which occurs in the catalyst layer and the membrane. Potential fields in these two media are described as follows.

For electrons:



$$\nabla \cdot (\sigma_{eff} \nabla \phi_e) + S_{\phi_e} = 0 \quad (2.27)$$

$$S_{\phi_e} = \begin{array}{ll} -j_a & \text{At anode} \\ j_c & \text{At cathode} \end{array} \quad (2.28)$$

For protons:

$$\nabla \cdot (\kappa_{eff} \nabla \phi_p) + S_{\phi_p} = 0 \quad (2.29)$$

$$S_{\phi_p} = \begin{array}{ll} j_a & \text{At anode} \\ -j_c & \text{At cathode} \end{array} \quad (2.30)$$

where  $\sigma_{eff}$ ,  $\kappa_{eff}$ ,  $\phi_e$ ,  $\phi_p$ ,  $S_{\phi_e}$  and  $S_{\phi_p}$  denote electron conductivity, proton conductivity, electronic phase potential, electrolyte phase potential, and consumption rates of charge and product in the electrochemical reaction in the catalyst layer, respectively.



The membrane conductivity is strongly related to the temperature and the water content  $\lambda$ . It is defined as the ratio of the number of water molecules to the number of charge sites [4]:

$$\kappa_{eff}(T) = (0.5139\psi - 0.00326) \exp \left[ 1268 \left( \frac{1}{303} - \frac{1}{T} \right) \right] \quad (2.31)$$

The water content of the membrane surface depends on the activity of the water vapor, which also depends on the partial pressure of the water. Therefore, the empirical relationship between them can be applied:

$$\psi = \begin{cases} 0.043 + 17.81a - 39.85a^2 + 36.0a^3 & 0 \leq a \leq 1 \\ 14 + 1.4(a - 1) & 1 < a \leq 3 \end{cases} \quad (2.32)$$

$$a = \frac{x_w P}{P_{sat}} \quad (2.33)$$

## 2.4 Boundary Conditions

Boundary conditions are necessary and crucial for solving the above equations. They describe the operating conditions as well as the model geometry characteristic of the PEM fuel cell. Due to the single-domain formulation, boundary conditions are required only at the external surfaces of the computational domain. The most important ones are as follows.

*Inlet boundaries:* The fuel and oxidant flow rates along the flow channel can be described by a stoichiometric flow ratio,  $\xi$ , which is defined as the ratio of the amount of reactant supplied to the amount of reaction to generate the specified reference current density  $I_{ref}$ . [37]. At the gas channel, the temperature and gas species concentrations are assumed to be uniform. The inlet velocities are specified by

$$u_{a,in} = \xi_a \frac{I_{ref}}{2F} A_m \frac{RT_{a,in}}{P_{a,in}} \frac{1}{x_{O_2}} \frac{1}{A_{ch}} \quad (2.34)$$

$$u_{c,in} = \xi_c \frac{I_{ref}}{4F} A_m \frac{RT_{c,in}}{P_{c,in}} \frac{1}{x_{H_2}} \frac{1}{A_{ch}} \quad (2.35)$$

Where  $\xi_a$  and  $\xi_c$  are the reactant stoichiometric flow ratio of anode and cathode,


respectively.  $A_m$  is the geometrical area of the membrane and  $A_{ch}$  is the cross-sectional area of the gas channel.

*Outlet boundaries:* Fully developed flow is applied. At the outlets, both anode and cathode channels assumed sufficiently long so that velocity and species concentration fields are fully developed.

*Walls:* Neumann conditions and no-slip conditions are applied.

*Symmetric boundaries:* Mass flux or momentum flux have zero gradients.

*Electronic phase potential boundaries:* Fixed total cell overpotential at the outer boundary of the cathode is specified.



$$\left\{ \begin{array}{ll} \phi_e = 0 & \text{at anode bipolar plate} \\ \phi_e = \eta_{cell} & \text{at cathode bipolar plate} \\ \frac{\partial \phi_e}{\partial y} = 0 & | \text{ otherwise} \end{array} \right. \quad (2.36)$$

The cell potential can be obtained from the following expression

$$V_{cell} = V_{oc} + \eta_{tot} \quad (2-37)$$

where  $\eta_{tot}$  and  $V_{oc}$  are total cell overpotential and pen circuit voltage, respectively

[17].

$$V_{oc} = 0.2329 + 0.0025T \quad (2-38)$$

## 2.5 Numerical Procedures

### 2.5.1 Numerical Method

The solution to the governing equations is performed by employing a finite volume scheme with the model domain divided into a number of cells as control volumes. The governing equations are numerically integrated over each of these computational cells or control volumes. The method exploits a collocated cell-centered variable arrangement with the local or cell-averaged values of the physical quantities evaluated and stored at each cell center.

The governing equations can be expressed in the form of a generalized convection-diffusion type of transport equation:


$$\nabla \cdot (\rho \vec{u} \varphi - \Gamma_{\varphi} \nabla \varphi) = S_{\varphi} \quad (2-39)$$

where  $\varphi$  denotes the general dependent variable,  $\Gamma_{\varphi}$  the exchange coefficient,  $S_{\varphi}$  the source term,  $\vec{u}$  velocity vector, and  $\rho$  the density. With the discretization of the governing equations, the coupled finite-difference equations can be expressed in the form of

$$a_P \varphi_P = a_E \varphi_E + a_W \varphi_W + a_N \varphi_N + a_S \varphi_S + S_{\varphi} \quad (2-40)$$

where  $\varphi_P$  is the value of  $\varphi$  at the current point  $P$ ,  $\varphi_E \dots \varphi_S$  stand for the values of the grid points adjacent to the point  $P$ , and  $a_P \dots a_S$  are known as the link coefficients.

### 2.5.2 Calculation Procedure

The governing equations with their related boundary conditions are solved using a commercial code based on the SIMPLE algorithm for convection-diffusion problems. The numerical flow diagram of present investigation is shown in Fig. 2.2. As a convergence criterion it is imposed that the normalized residual for each model variable is smaller than  $10^{-4}$  [43].

### 2.5.3 Model Validation

In the simulation, a uniform grids distribution is used to calculate the complex electrochemical reaction and physical phenomena in the fuel cell. Three mesh systems- 41 x 13 x 47, 51 x 16 x 58, and 61 x 21 x 67 are constructed to explore numerical result dependence on computational cell numbers. Table 2.1 presents geometrical and operating parameters of the base model in the PEM fuel cell. The results of the polarization curve by the base model under different grid systems are shown in Fig. 2.3. Considering both accuracy and economics, the grid system of 51 in the z-direction, 16 in the x-direction, and 58 in the y-direction was selected for present research.

To further check the adequacy of the numerical scheme, it is clearly seen from Fig. 2.4 that the present predictions agree reasonably with the experimental data of Squadrito *et al.* [44]. The above preliminary runs confirm that the present model and

the numerical method used are generally appropriate in analysis of the present problem.



Table 2.1. Geometrical and operating parameters

Quantity	Value	Sources
Gas channel depth/width	0.762 / 0.762 mm	
Shoulder width	0.381 mm	
GDL thickness	0.3 mm	
Catalyst layer thickness	0.01 mm	
Membrane thickness	0.03 mm	
Fuel cell height/length	1.534 / 71.12 mm	
Anode/cathode pressure	1 / 1 atm	
Stoichiometry, at $\xi_a / \xi_c$ at $1.0 \text{ A/cm}^2$	1.5 / 3	[44]
Relative humidity of anode/cathode inlet	100 / 100 %	
Porosity of diffusion and catalyst layers	0.4 / 0.4	[45]
Porosity of membrane	0.28	[45]
Permeability of diffusion and catalyst layers	$1.76 \times 10^{-11} / 1.76 \times 10^{-11} \text{ m}^2$	[14]
Permeability of membrane	$1.8 \times 10^{-18} \text{ m}^2$	[14]
Transfer coefficient at anode/cathode	0.5 / 1.5	[14]
Condensation rate constant	$100 \text{ s}^{-1}$	[17]
Evaporation rate constant	$100 \text{ atm}^{-1} \text{ s}^{-1}$	[17]
Tortuosity of the diffusion and catalyst layers	1.5	[14]
Tortuosity of the membrane	3	[14]
Surface tension, $\zeta$	$0.0625 \text{ Nm}^{-1}$	[41]

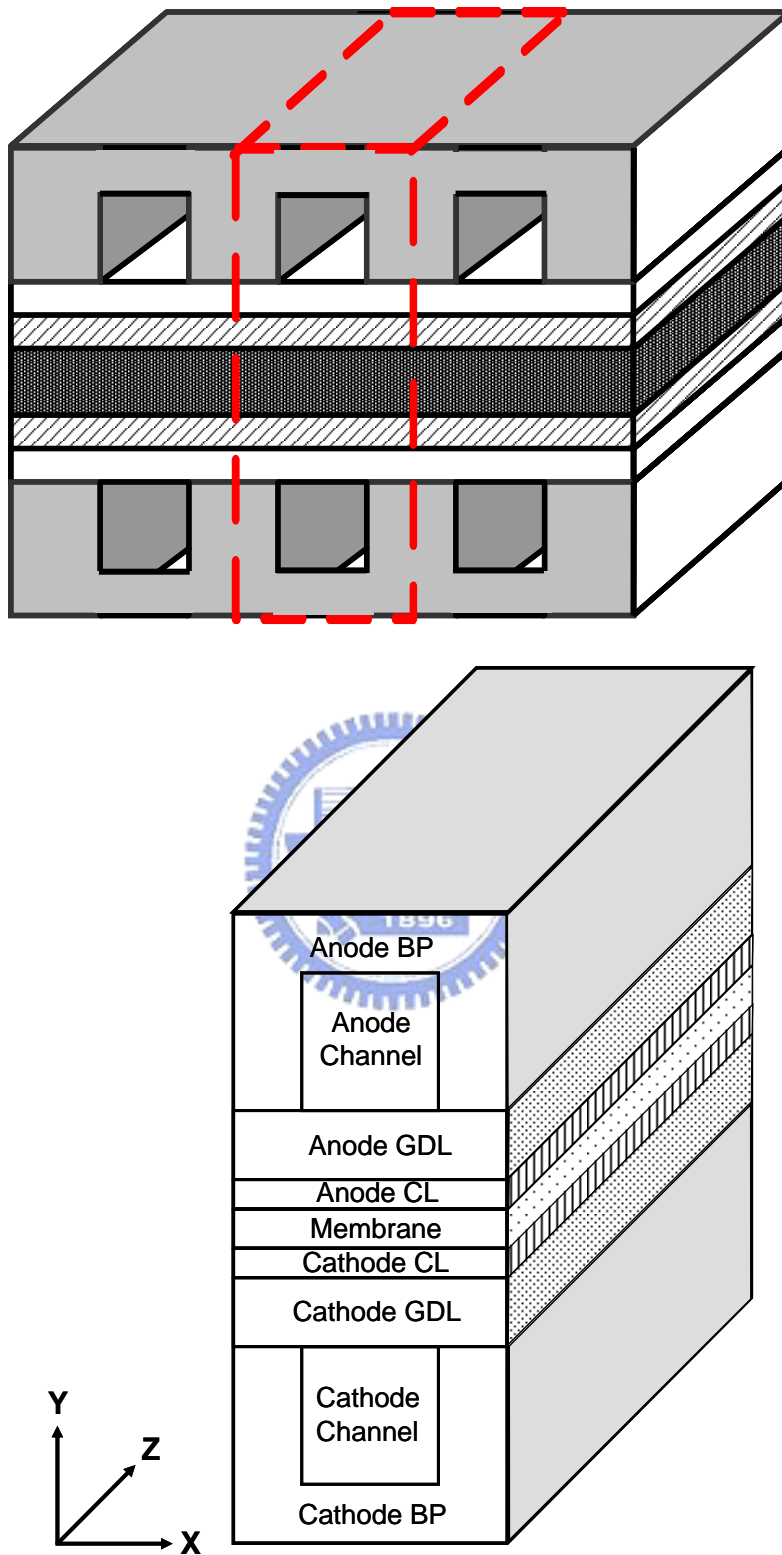


Figure 2.1 Physical and computational domains considered in this study



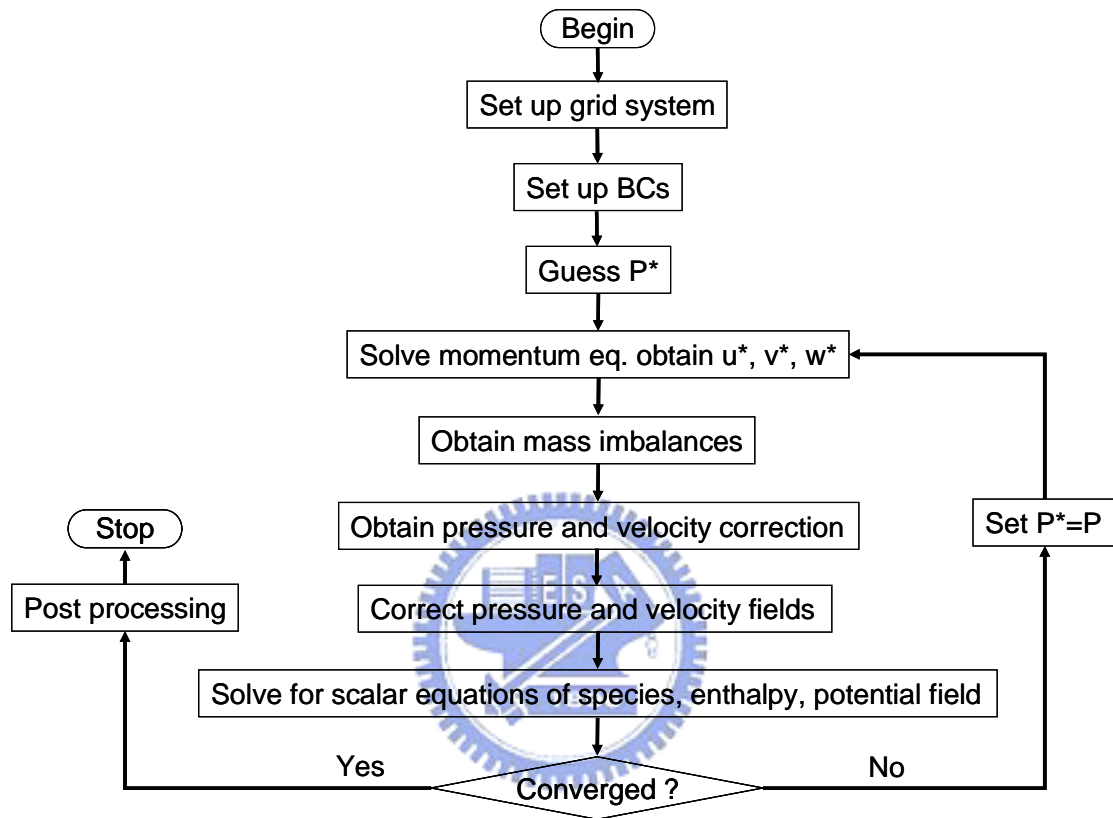


Figure 2.2 Numerical flow diagram of the solution procedure.

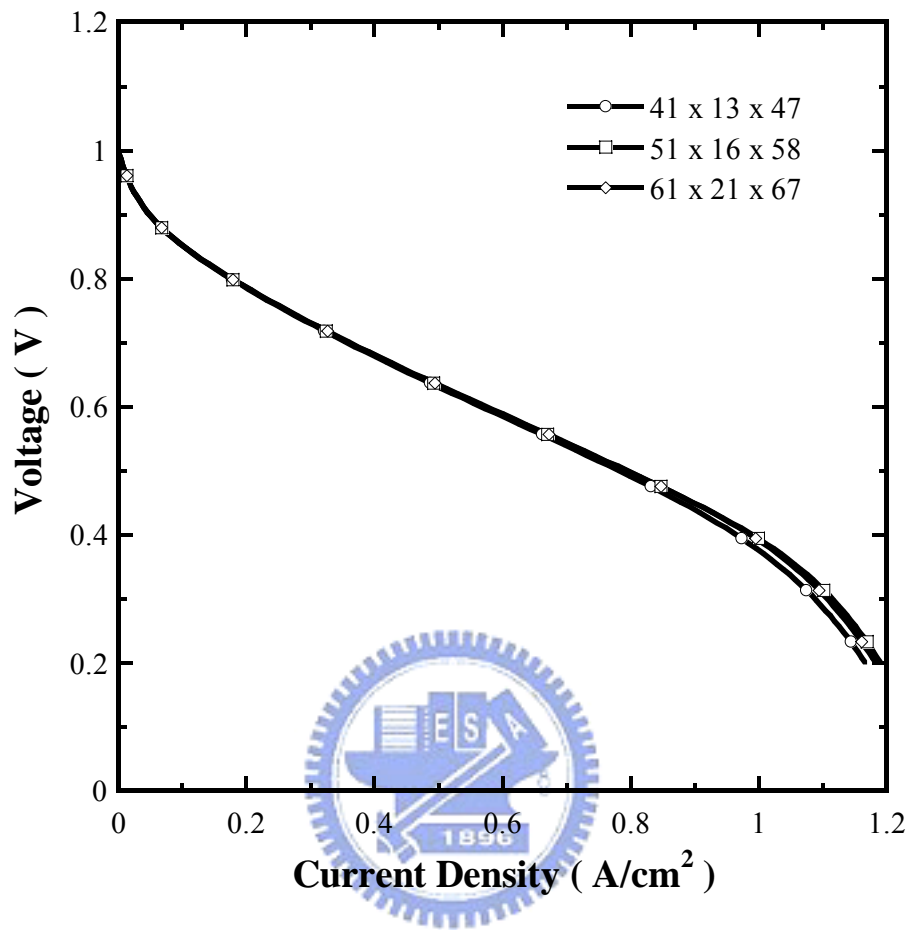


Figure 2.3 Comparison of predictions on the three different grid systems.

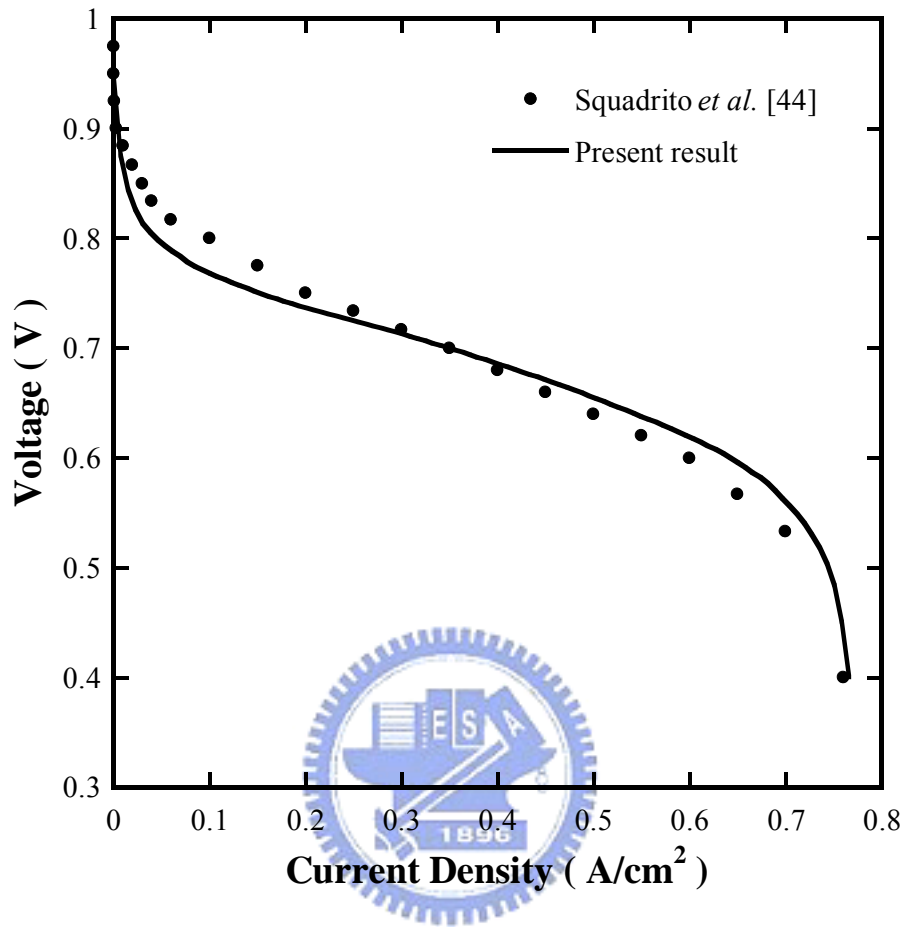


Figure 2.4 Comparison of the predicted  $I$ - $V$  curve and the experimental data of Squadrito *et al.* [44].

## CHAPTER 3

### EFFECTS OF CATHODE HUMIDIFICATION AND POROSITY OF THE GDL ON THE GAS-LIQUID INTERFACE LOCATION IN A PEM FUEL CELL

#### 3.1 *Introduction*

A PEM fuel cell is prone to gas-liquid two-phase formation due to its low operating temperature, particularly under highly humidified or high current density conditions. When the gas diffusion layer and the catalyst layer become saturated with water vapor, the product water starts to condense and block open pores, reducing the available paths for oxygen transport. This phenomenon is termed “flooding” and becomes a major limiting factor of PEM fuel cell performance. Hence, it is critical to understand the two-phase flow and transport in a PEM fuel cell, and a mathematical model is useful to improve this understanding. In practice, humidification of anode fuels and/or cathode oxidants is often used to provide sufficient membrane hydration. Since water is generated in the cathode catalyst layer from electrochemical reaction and it also tends to migrate from the anode side to the cathode side by the electro-osmotic drag, it becomes a key issue in the design and operation of PEM fuel cells to avoid the flooding phenomenon in the cathode. In this chapter, effects of

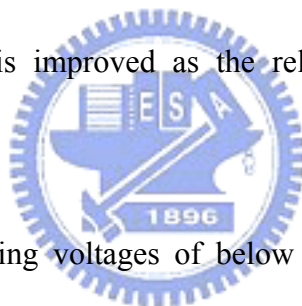
cathode humidification and gas diffusion layer porosity on the gas-liquid interface location in a PEM fuel cell are investigated and described in detail. For all of the calculations carried out in this study, the fuel flows were co-flows and inlet stoichiometric ratios of 1.5 and 3 are used for the anode and cathode sides based on a reference current density of  $1 \text{ A/cm}^2$ . The inlet fuel, hydrogen, is assumed to be fully humidified on the anode-side; the cell temperature and humidification temperature are 343 K and the operating pressure is 1 atm.

### ***3.2 Effects of cathode humidification scheme***

In this study, the location of the gas-liquid interface along the flow channel direction at various cathode humidity conditions and its effect on cell performance are elucidated by modeling a three-dimensional PEM fuel cell system using CFD. Figure 3.1 shows the effect of the relative humidity of the cathode on the location of the interface where the liquid water begins to condense along flow channel at a cell operating voltage of 0.7 V. The interface is defined as the location where liquid water begins to condense. The horizontal dotted line indicates the interface between the flow channel and the gas diffusion layer. A higher cathode relative humidity corresponds to a smaller distance between the gas-liquid interface and the gas inlet, as clearly displayed in Fig. 3.1 (a). Furthermore, the gas-liquid interface location moves to the

flow channel inlet region as the relative humidity of the cathode increases. This phenomenon is caused by: (i) the decrease in the amount of evaporated water through the flowing gas stream; (ii) the increase in the partial pressure of water and the ability to reach the saturation pressure of the vapor water relatively quickly to form liquid water earlier as the relative humidity of the cathode increases. On the contrary, the gas-liquid interface location moves closer to the cathode catalyst layer when the relative humidity of the cathode is less than 60%, as shown in Fig. 3.1 (b). In conclusion, increasing the relative humidity of the cathode can reposition the gas-liquid interface and cause liquid water to appear, affecting the performance of the cell, because liquid water may occupy the pores in the porous media, reducing the amount of fuel gas that can reach the cathode catalyst layer. Figures 3.2 (a) and 3.2 (b) plot  $I-V$  and  $I-P$  curves at various relative humidity of the cathode with conventional flow fields. The results in Fig. 3.2 (a) reveal that the cell performance decreases as the relative humidity of the cathode increases, because the amount of liquid water increases with the relative humidity. Accordingly, the pores in the porous media were obstructed by liquid water at the cathode-side, reducing the amount of reaction gas to the cathode catalyst layer. Therefore, the performance of the cell gradually decreases. Also, the polarization curves do not seem to vary as the relative humidity of the cathode increases, at an operating voltage that exceeds  $\sim 0.65$  V. A large voltage results

in a small current density, and therefore, a relatively small electrochemistry reaction rate. However, the performance of the cell decreases significantly as the operating voltage declines below the  $\sim 0.65$  V operating voltage, since the large current density accelerates the rate of the electrochemical reaction. In particular, in Fig. 3.2 (a), the higher cathode relative humidity (100%) offers a better cell performance than the lower one (20%) at an operating voltage of over  $\sim 0.65$  V, because the rate of the electrochemical reaction decreases as the operating voltage increases. Therefore, the water content of the membrane in the initial stage increases with the relative humidity. Thus, the cell performance is improved as the relative humidity of the cathode increases.

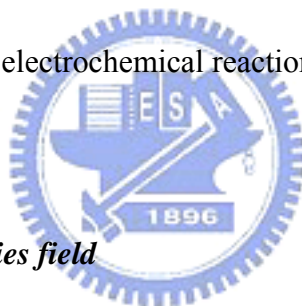


By contrast, at operating voltages of below  $\sim 0.65$  V, the cell performance improves as the relative humidity of the cathode decreases, because accelerating the electrochemical reaction produces more water, increasing the water content in the membrane at a low cathode relative humidity, such as 20%. However, at high relative humidity, flooding may occur at the cathode-side. Additionally, the power density increases as the relative humidity of the cathode decreases, as shown in Fig. 3.2 (b).

### ***3.3 Effects of cell operating voltage***

Figure 3.3 shows the effects of various operating voltages on the location of

the gas-liquid interface along the flow channel at a relative humidity of the cathode of 80%. Figure 3.3 reveals that the gas-liquid interface location is close to the cathode catalyst layer at high operating voltage, indicating that less water was generated at a lower electrochemical reaction rate. However, since more water is generated at a high electrochemical reaction rate, the gas-liquid interface location is close to the gas diffusion layer and the flow channel at a low operating voltage. In closing, the gas-liquid interface location gradually moves to the gas channel inlet region as the operating voltage decreases, because reducing the operating voltage increases the current density. Therefore, the electrochemical reaction rate increases.



#### ***3.4 Three-dimensional species field***

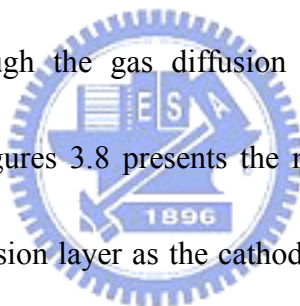
Figures 3.4 and 3.5 plot the oxygen and water fractions in the gas flow channel and the gas diffusion layer, respectively, of the cathode-side in the direction of the flow channel at an operating voltage of 0.7 V and relative humidity of the cathode at 80%. Larger oxygen fraction appears in the gas channel inlet region, and then gradually decreases in the flow channel direction, as shown in Fig. 3.4. The results reveal that the decrease in the oxygen fraction is caused by the catalyst layer consuming more oxygen on the cathode-side. Hence, the oxygen fraction is lowest near the cathode catalyst layer. By contrast, Fig. 3.5 reveals that the water fraction



gradually increases along the flow channel direction, because of the production of water in the catalyst layer of the cathode by the electrochemical reaction, as well as the transport of water from the anode-side to the cathode-side by electro-osmotic drag. Accordingly, the water fraction is the highest near the cathode catalyst layer. Since the water mass fraction is higher near the cathode catalyst layer, where the corresponding water partial pressure exceeds the saturated vapor pressure, causing the formation of liquid water. Therefore, Fig. 3.6 shows the liquid water saturation field in the gas channel and the gas diffusion layer of the cathode-side at an operating voltage of 0.7 V and a relative humidity of the cathode of 80%. The figure shows that saturation of the liquid water increases along the flow channel direction, because the electrochemical reaction causes the partial pressure of the water to exceed the saturated vapor pressure, causing liquid water to condense. The capillary force also causes liquid water to move toward the gas diffusion layer. Hence, this interface is the single-phase region when the saturation of the liquid water is zero. It becomes a two-phase region when the saturation of the liquid water exceeds zero. According to Fig. 3.1, to the right of the point where water condensation starts, a two-phase region is present along the flow channel direction. A single-phase region exists on the other side.

Figures 3.7 show that the oxygen mass fraction contours at the cathode gas

diffusion layer as the cathode humidification of (a) 20% (b) 60% (c) 100% for cell voltage of 0.4 V. It is obvious from these plots that the oxygen mass fraction gradually decreased along the flow channel direction from the inlet toward outlet owing to the consumption of oxygen by the electrochemical reaction in the cathode catalyst layer. This figure also shows that the oxygen mass fraction decreases as the cathode humidification increases from the 20% to 100%. This is attributed to the fact that a higher relative humidity of cathode causes greater amount of water vapor enters the electrode; therefore more liquid water is apt to condense in the pore space. Hence, the amount of the oxygen through the gas diffusion layer is reduced and the cell performance is decreased. Figures 3.8 presents the mass fraction contours of water vapor at the cathode gas diffusion layer as the cathode humidification of (a) 20% (b) 60% (c) 100% for cell voltage of 0.4 V. The results reveal the fact that water fraction gradually increases along the flow channel direction owing to the production of water in the cathode catalyst layer by the electrochemical reaction. Also the water concentration increases in the gas diffusion layer as the cathode humidification increases. The distributions of the liquid water saturation for these cases are showed in Fig 3.9. From these figures, it is found that when the cathode humidification is 20%, the amount of the liquid water in the gas diffusion layer is almost very small. However, when the cathode humidification is 100%, the there is some liquid water



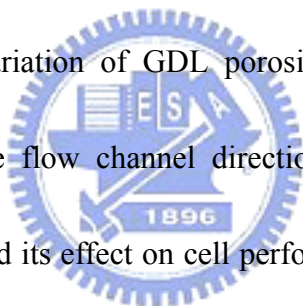
appears in the gas diffusion layer. Hence, the pores in the gas diffusion layer were obstructed by liquid water, reducing the amount of oxygen to the cathode catalyst layer. Therefore, it supports the argument of previous plot, namely, the oxygen mass fraction decreased owing to the blocking of liquid water in the pore of the porous media as the cathode humidification increases.

### ***3.5 Two-phase mixture velocity field***

Figure 3.10 shows the velocity field of the two-phase mixture in the gas diffusion layer and flow channel of the cathode at the cell voltage of 0.7 V and cathode relative humidity of 80%. As expected, there is a large difference in the velocity scale between the gas diffusion layer and the flow channel. The mixture velocity in the gas diffusion layer is at least two orders of magnitude smaller than that in the flow channel, indicating that gas diffusion is the dominant transport mechanism in the porous media. The flow field in the flow channel is fully developed in view of the large aspect ratio of the channel length to height (equal to 93 in the present study), as can be seen from Fig. 3.7 where the channel length is, however, not drawn to scale for better view.

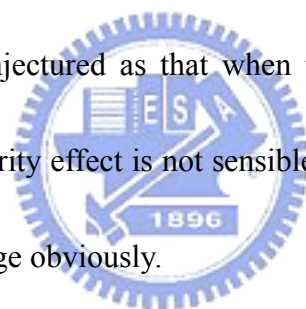
### ***3.6 Effects of the cathode gas diffusion layer porosity***

The porosity of the cathode gas diffusion layer has two different effects on the fuel cell performance: as the porous region provides the space for the reactants to diffuse towards the catalyst layer region, an increase in the porosity means that the onset of mass transport limitations occurs at higher current densities, *i.e.* it leads to higher limiting currents. The adverse effect of a high porosity is an expected increase in the contact resistance. Contact resistance occurs at all interfaces inside the fuel cell, the most important one being the interface between the bipolar plates and the gas diffusion layers. In this study, the solid phase conductivity is assumed constant and does not change with the variation of GDL porosity. Hence, the location of the gas-liquid interface along the flow channel direction at various porosities of the cathode gas diffusion layer and its effect on cell performance were elucidated. Figure 3.11 shows the effects of the cathode gas diffusion layer porosity on the location of the gas-liquid interface where the liquid water begins to condense along flow channel direction at a cell voltage of 0.7 V and a relative humidity of the cathode of 80%. The results in Fig. 3.11 show that the location of the gas-liquid interface appears early and is closed to the flow channel inlet region in the gas diffusion layer as the gas diffusion layer porosities decreased. These phenomena can be explained as that given smaller porosity of the gas diffusion layer, the liquid water is more difficult to transport out of the gas diffusion layer, hence, the liquid water will spread throughout the gas



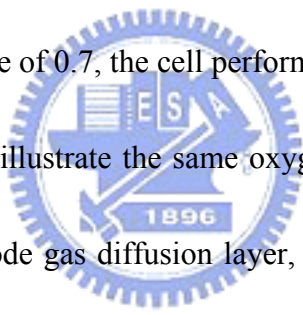
diffusion layer. Once the liquid water block the pores of the porous media, causing the hinder the diffusion transport of fuel gas to the cathode catalyst layer, thus limiting the electrochemical reaction and causing the decrease of cell performance. On the contrary, the higher porosity of the cathode gas diffusion layer facilitates the transport of water from the cathode catalyst layer to the flow channel. Hence, less water blocks the pores of the gas diffusion layer, increasing the vacant pores space and helping the reactant diffusion to the cathode catalyst layer. Nevertheless, the variation of the gas-liquid interface location becomes small as the porosity changes from 0.7 to 0.8.

The phenomenon can be conjectured as that when the cathode gas diffusion layer porosity is too big, the capillarity effect is not sensible, hence, the gas-liquid interface location doesn't seem to change obviously.



Figures 3.12 (a) and 3.12 (b) show  $I-V$  and  $I-P$  curves at various porosities of the cathode gas diffusion layer at a relative cathode humidity of 80%. In Fig. 3.12 (a) the  $I-V$  curves demonstrate that a better performance can be obtained by using a gas diffusion layer of higher porosity. The remarkable drop in cell potential is caused by a mass transfer or concentration loss, which is a consequence of shortage of the reactant gas at high current density in which more reactant gas is required for fast reaction. A gas diffusion layer of higher porosity has an ability of stronger diffusion transport, which is beneficial in that it supplements the reactant gas to the cathode catalyst layer

and thus shifts the occurrence of the performance drop to a higher value of the current density. However, Fig. 3.12 (a) also shows that when the cathode gas diffusion layer porosity reaches the value of 0.8, the cell performance almost does not change comparing with the value of 0.7. This phenomenon also conform the result of Fig. 3.11. The variation of power density is also shown in Fig. 3.12 (b). It reveals that the power density increases with the cathode gas diffusion layer porosity. In closing, if the variation of solid phase conductivity is neglected, the cell performance is enhanced as the cathode gas diffusion layer porosity increase. But when the cathode gas diffusion layer porosity reaches the value of 0.7, the cell performance is not enhanced.



Figures 3.13 and 3.14 illustrate the same oxygen and water mass fractions at various porosities of the cathode gas diffusion layer, respectively, in the direction of the flow channel at an operating voltage of 0.7 V and a cathode relative humidity of 80%. According to the model equations, a higher porosity of gas diffusion layer accelerates the speed of oxygen diffusion to the cathode catalyst layer, as displayed in Fig. 3.13. Because of the aperture of the pores being relatively large, meaning that it may not block by the liquid water and the diffusion transport of reactant gas is easy to pass through the pores of gas diffusion layer. Hence, the oxygen does not spread throughout the gas diffusion layer, and can reach the cathode catalyst layer. On the contrary, the reactant gas spread throughout the gas diffusion layer for a small

porosity of gas diffusion layer. The diffusion transport of the reactant gas and the liquid water by the capillary force to pass through the gas diffusion layer is difficult. Fig. 3.13 also shows that when the porosity value is 0.7, no matter what the porosity is increased, the oxygen mass fraction does not change obviously because of the fuel gas or water almost pass through the gas diffusion layer directly. Figure 3.14 shows a similar result with Fig 3.13. That is, the water moves through the gas diffusion layer more easily at higher porosity of gas diffusion layer and the water does not remarkably occupy the pores and thus preventing the oxygen diffusion transport.

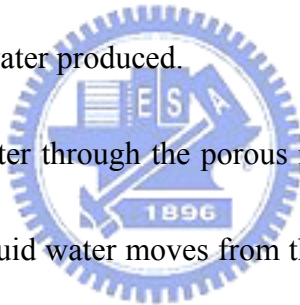
### 3.7 Summary



An isothermal, multi-dimensional, multi-component, computational fluid dynamic model was developed to study the effect of the cathode humidification conditions and the cathode gas diffusion layer porosities on the location of the interface where the liquid water begins to condense along the flow channel direction in a PEM fuel cell. The model results support the following conclusions.

- (1) The gas-liquid interface location moves from the cathode catalyst layer toward the gas diffusion layer as the relative humidity of the cathode increases. When the relative humidity of the cathode reaches 100%, the gas-liquid interface location is close to the gas flow channel inlet region.

- (2) As the condensed water in the pores in the porous media blocks the transport of fuel gas, the cell performance and power density decrease as the relative humidity of the cathode increases.
- (3) Reducing the cell operating voltage reduces the distance between the gas-liquid interface and the gas flow channel inlet region, because the higher current density is associated with a higher electrochemical reaction rate.
- (4) The decreased oxygen fraction and the increased water fraction along the flow channel are related to the electrochemical reaction of the cathode catalyst layer, as oxygen is consumed and water produced.
- (5) The transport of liquid water through the porous media is driven by the capillary force. Accordingly, the liquid water moves from the cathode catalyst layer toward the gas diffusion layer and the flow channel.
- (6) The diffusion transport of the reactant gas to the cathode catalyst layer and the production of water via the gas diffusion layer to the flow channel increases with increasing the cathode gas diffusion layer porosities. Consequently, the cell performance and power density are increased.





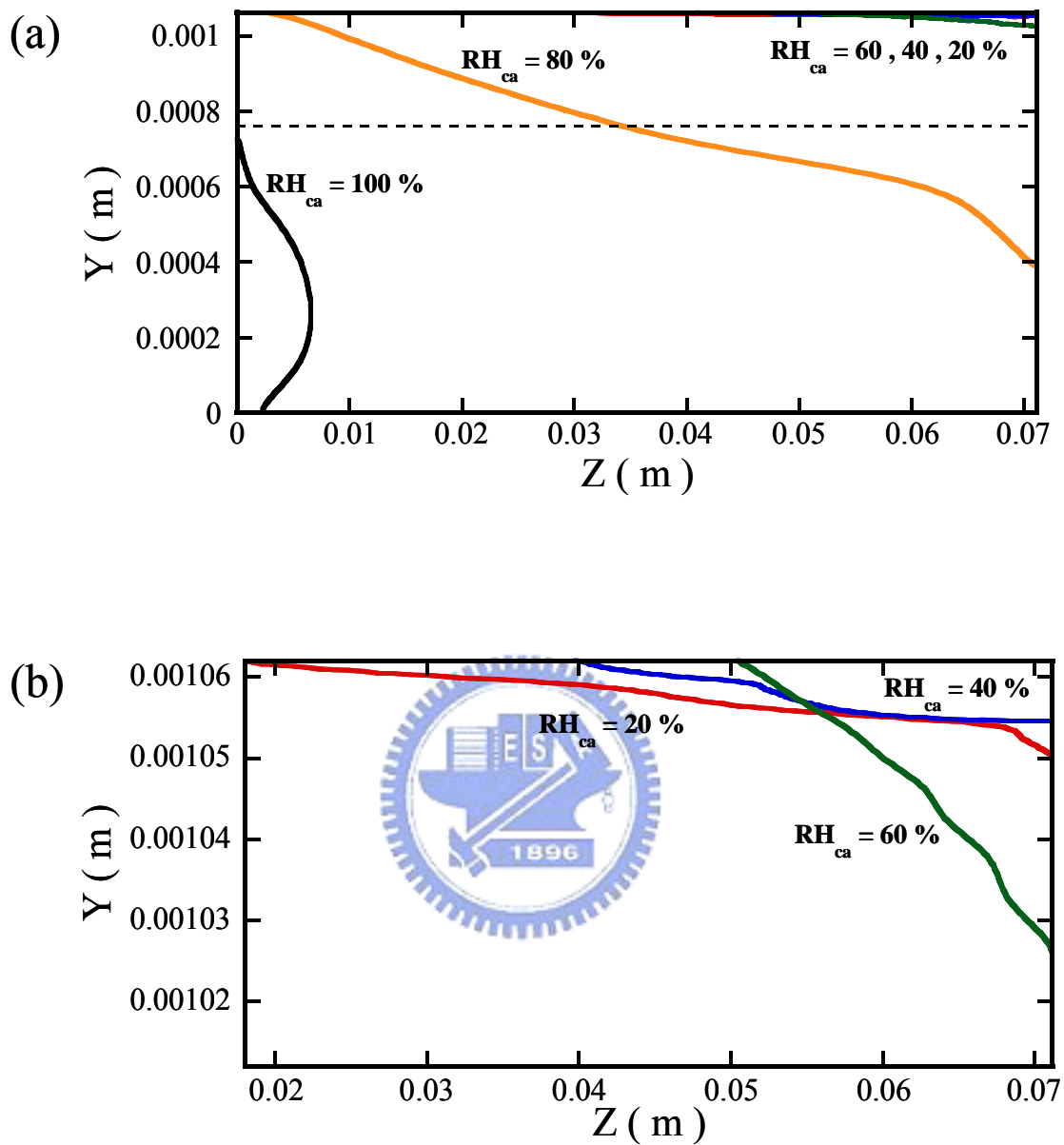


Figure 3.1 Effects of relative humidity of cathode on the location of the interface where liquid water begins to condense along the conventional flow channel at a cell operating voltage of 0.7 V. (a)  $RH_{ca} = 20\sim 100\%$  and (b)  $RH_{ca} = 20\sim 60\%$ .

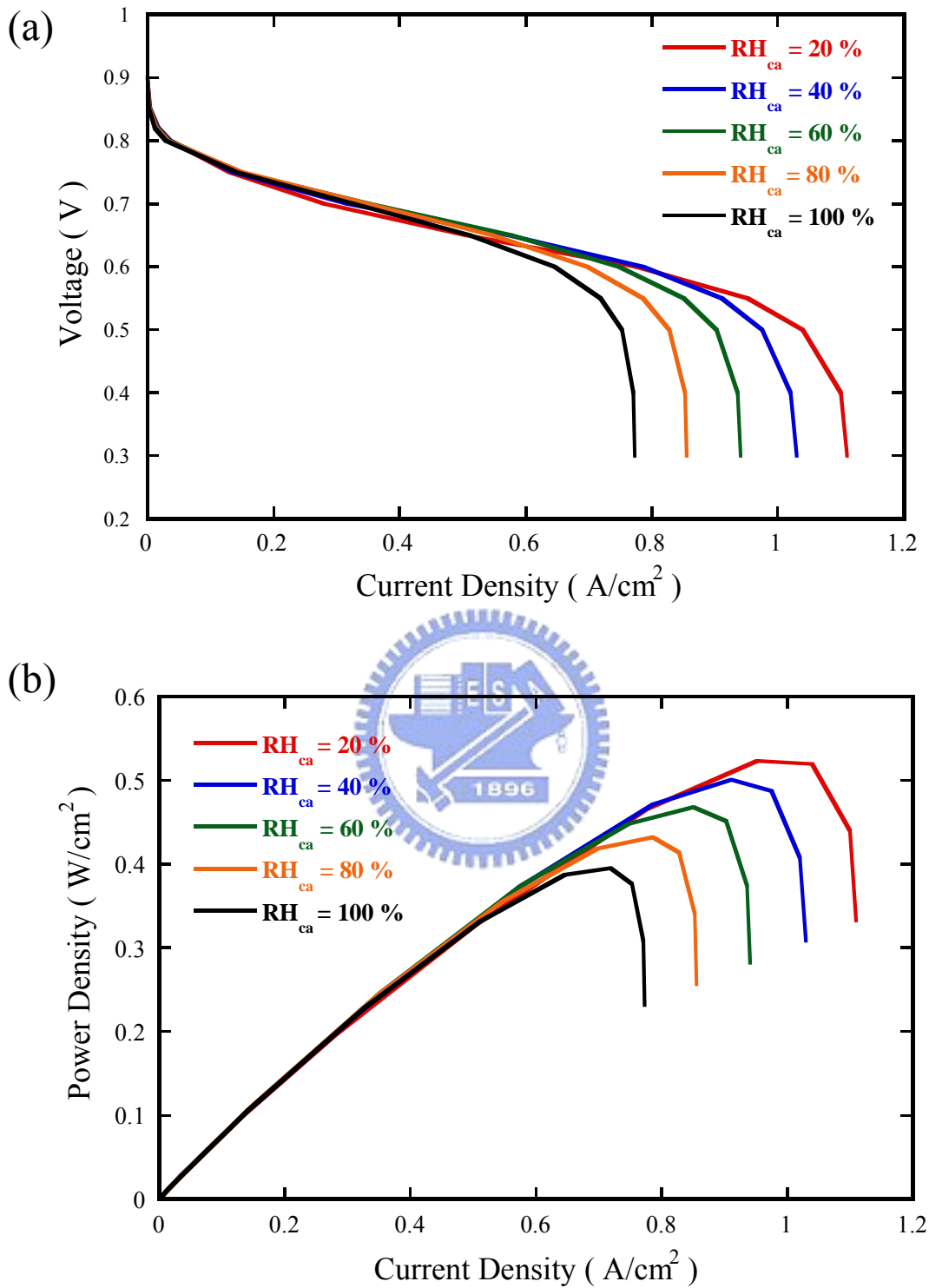


Figure 3.2 Effect of relative humidity of the cathode on cell performance with conventional flow fields. (a)  $I$ - $V$  curves and (b)  $I$ - $P$  curves.

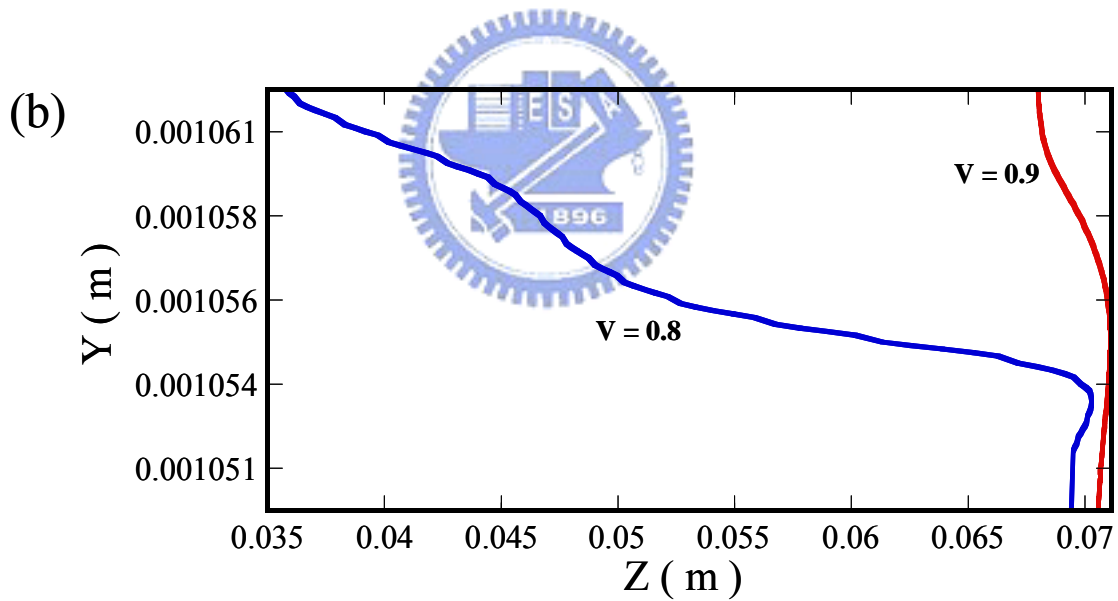
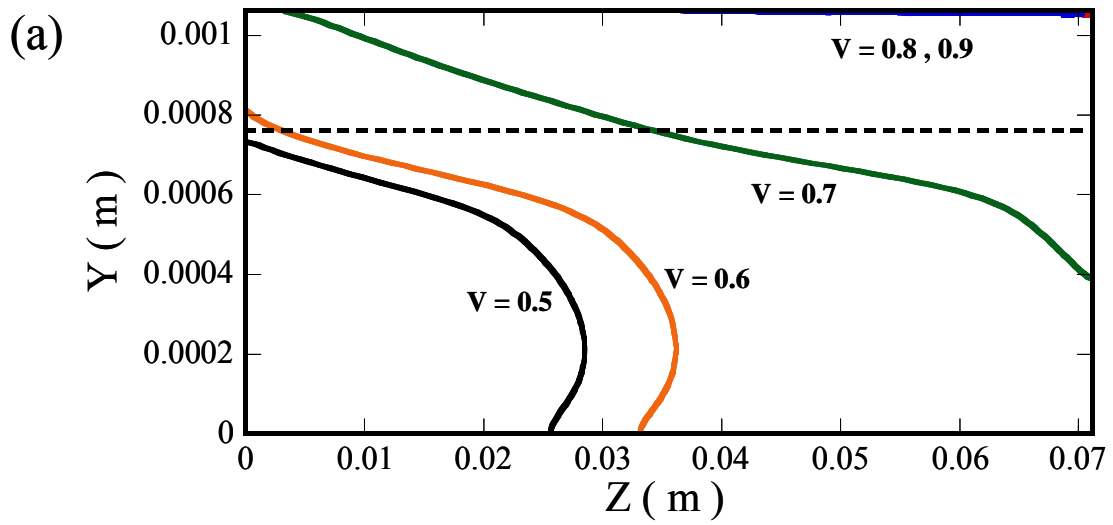


Figure 3.3 Effect of cell operating voltage on the location of the interface where liquid water begins to condense along the conventional flow channel at a relative humidity of the cathode of 80 %. (a)  $V = 0.5 \sim 0.9$  (b)  $V = 0.8 \sim 0.9$ .

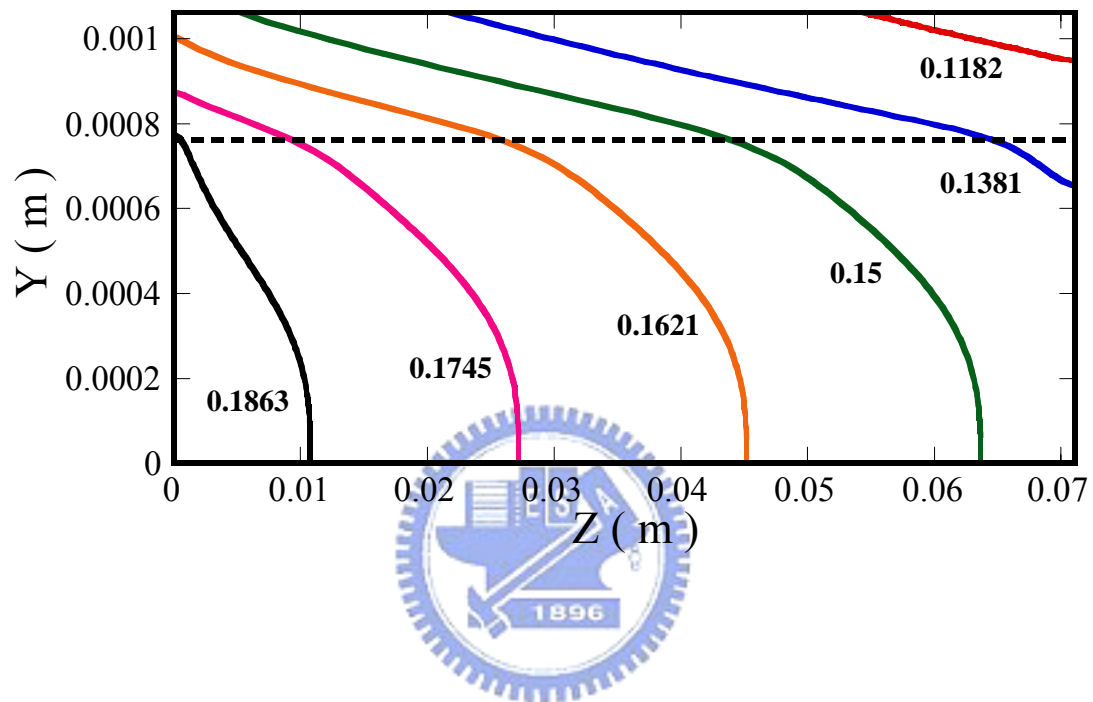


Figure 3.4 Oxygen fraction in the cathode gas channel and gas diffusion layer along the conventional flow channel at a cell voltage of 0.7 V and cathode relative humidity of 80 %.

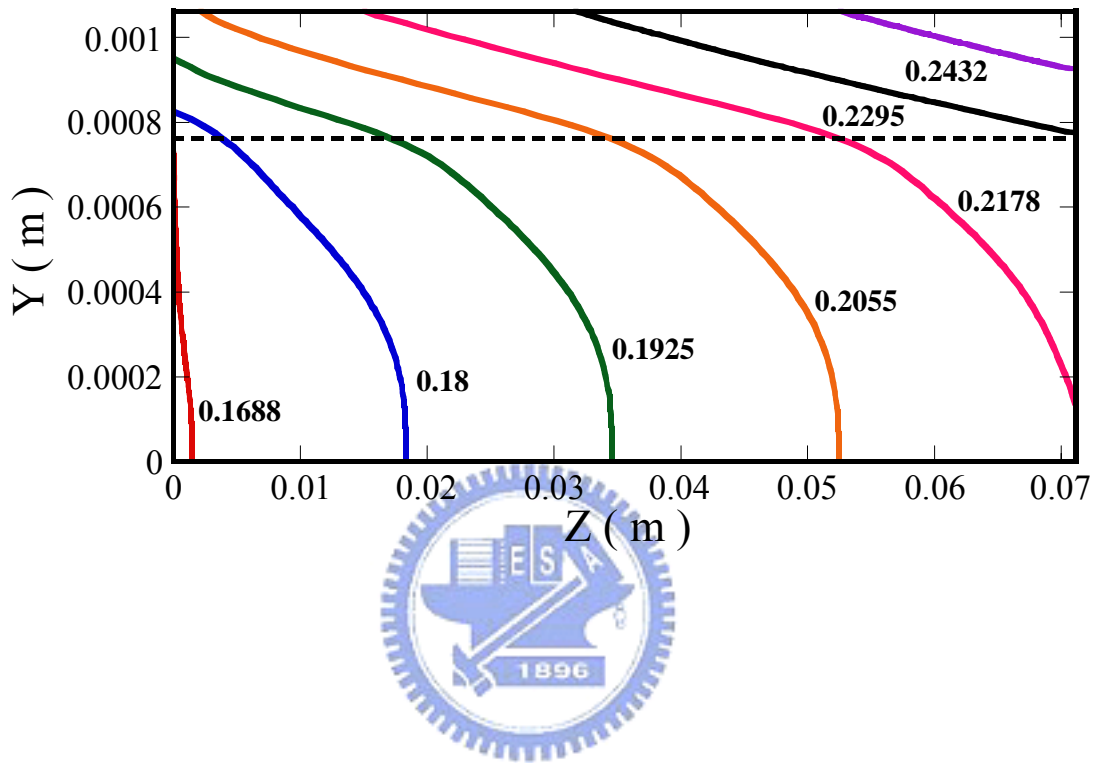


Figure 3.5 Water fraction in the cathode gas channel and the gas diffusion layer along the conventional flow channel at a cell voltage of 0.7 V and cathode relative humidity of 80 %.

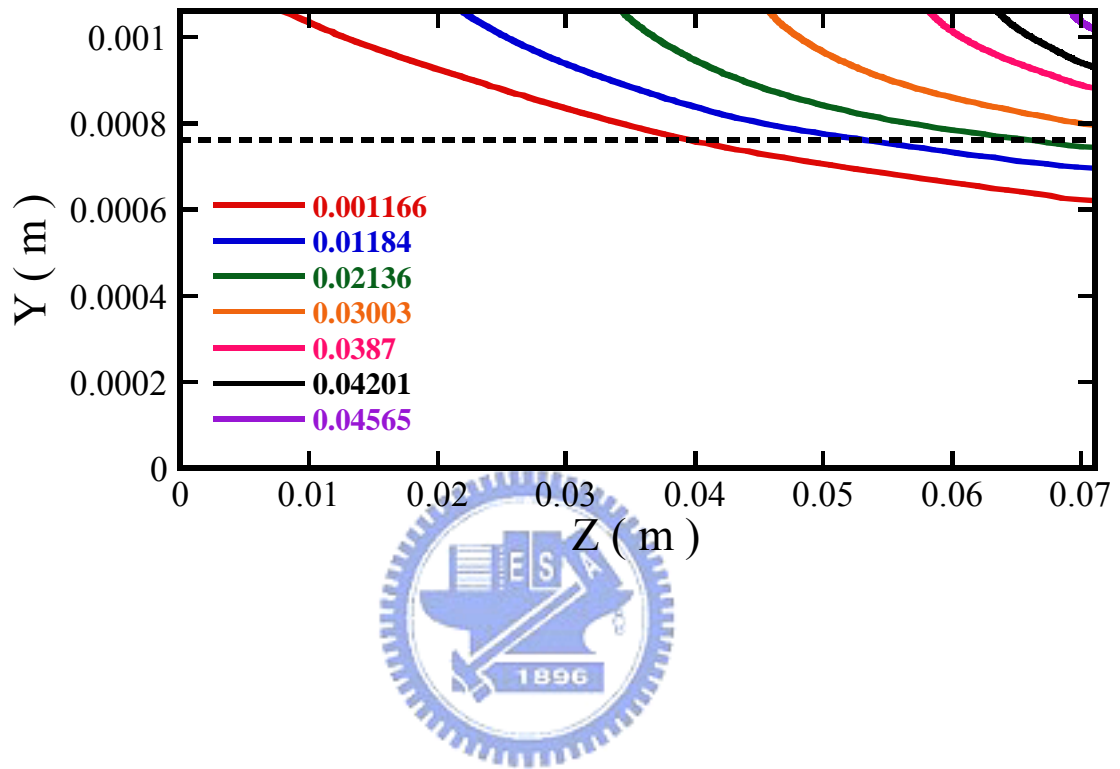


Figure 3.6 Liquid water saturation field in the cathode gas channel and gas diffusion layer along the conventional flow channel at a cell voltage of 0.7 V and cathode relative humidity of 80 %.

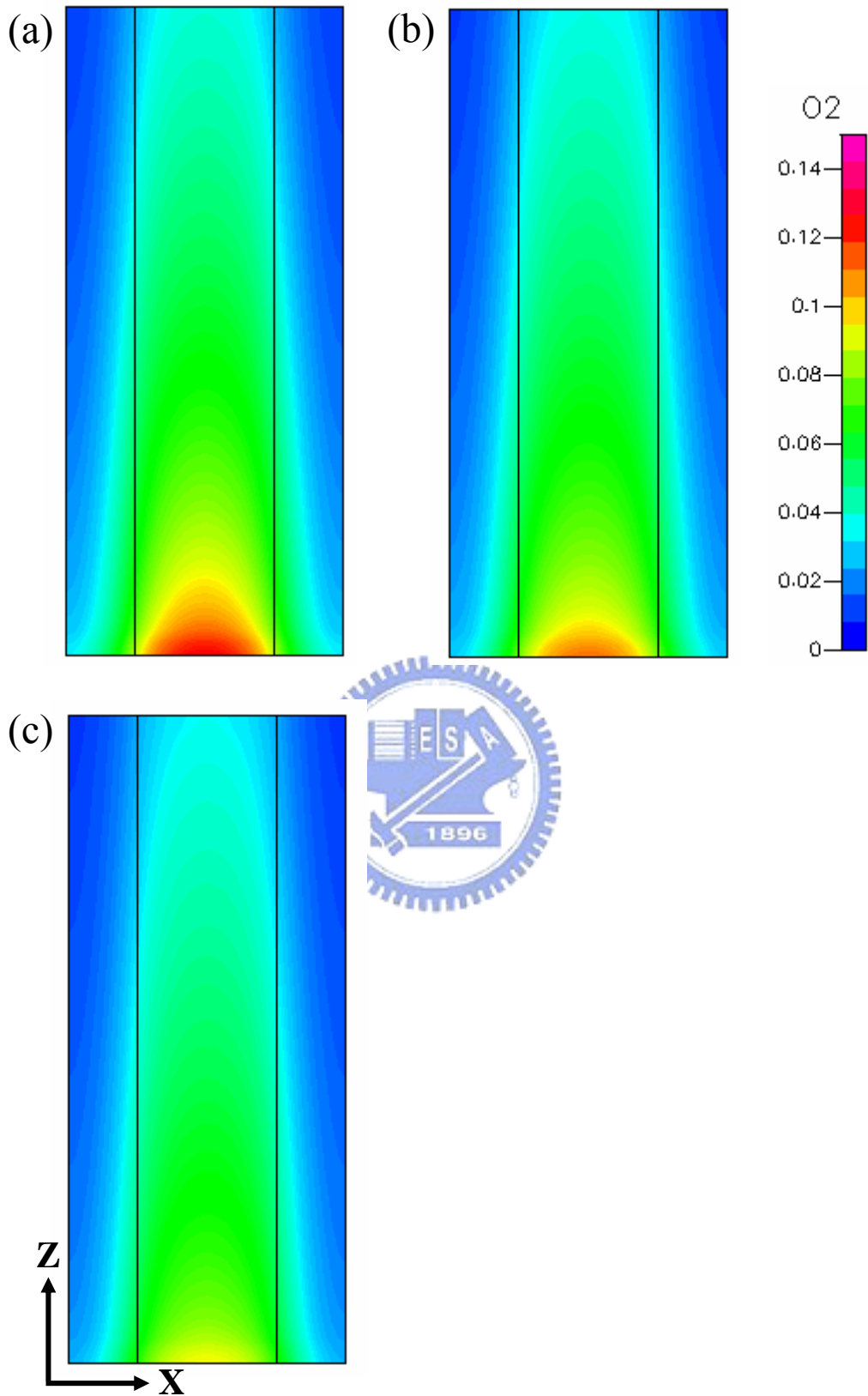


Figure 3.7 Oxygen mass fraction contours at the gas diffusion layer as the cathode humidification of (a) 20 % (b) 60 % (c) 100 % for cell voltage of 0.4 V.

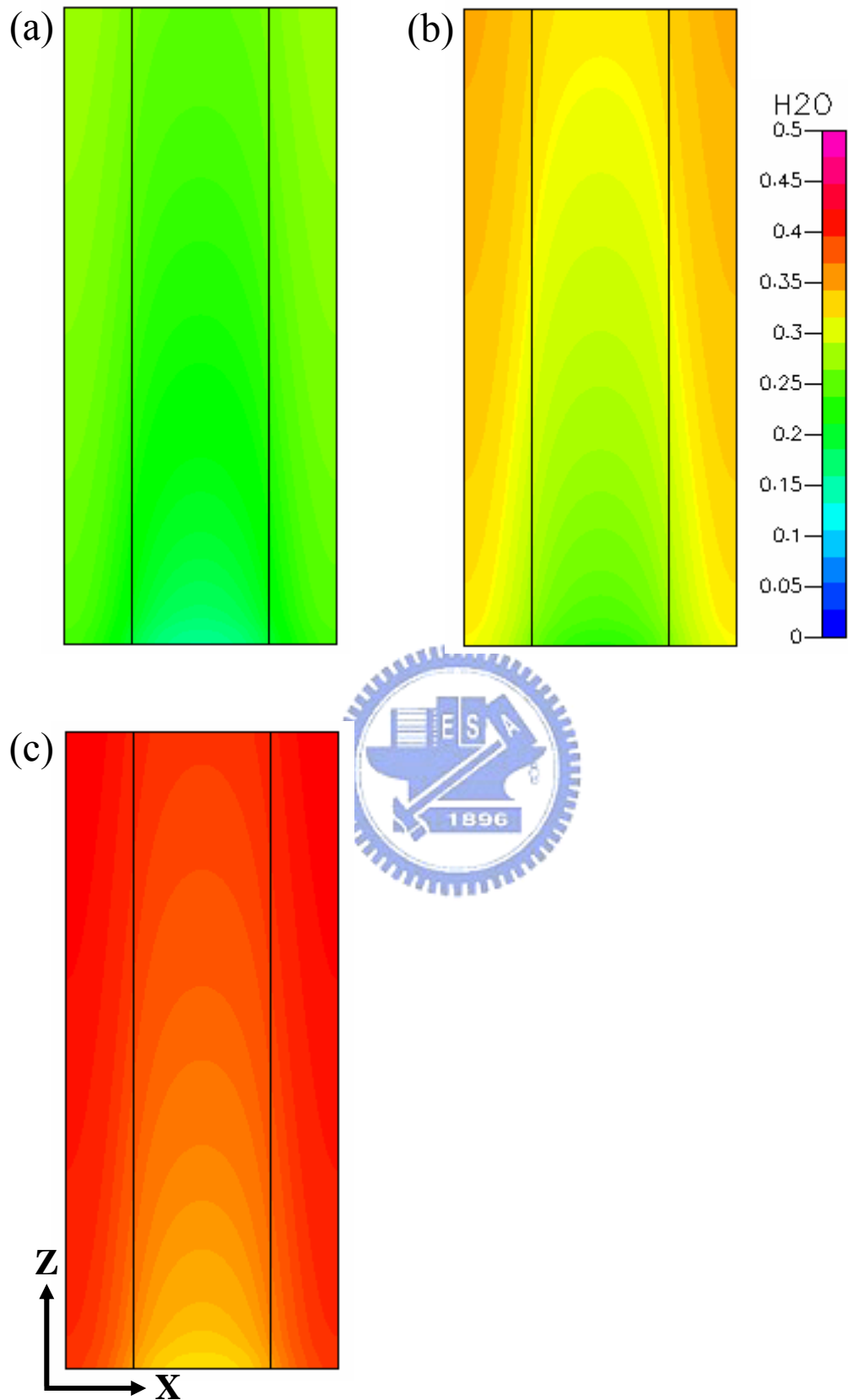


Figure 3.8 Water mass fraction contours at the gas diffusion layer as the cathode humidification of (a) 20 % (b) 60 % (c) 100 % for cell voltage of 0.4 V.



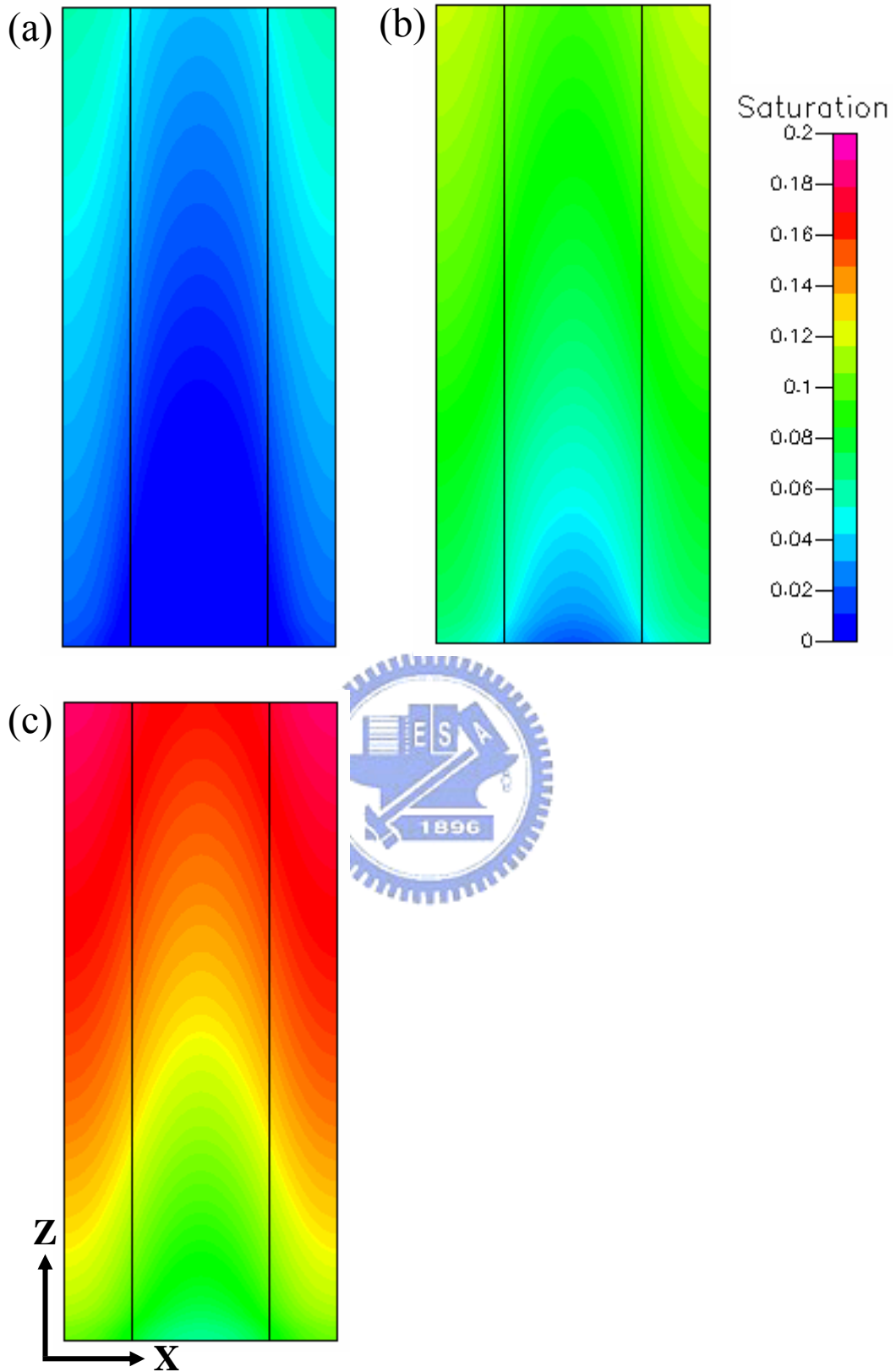


Figure 3.9 Liquid saturation contours at the gas diffusion layer as the cathode humidification of (a) 20 % (b) 60 % (c) 100 % for cell voltage of 0.4 V.

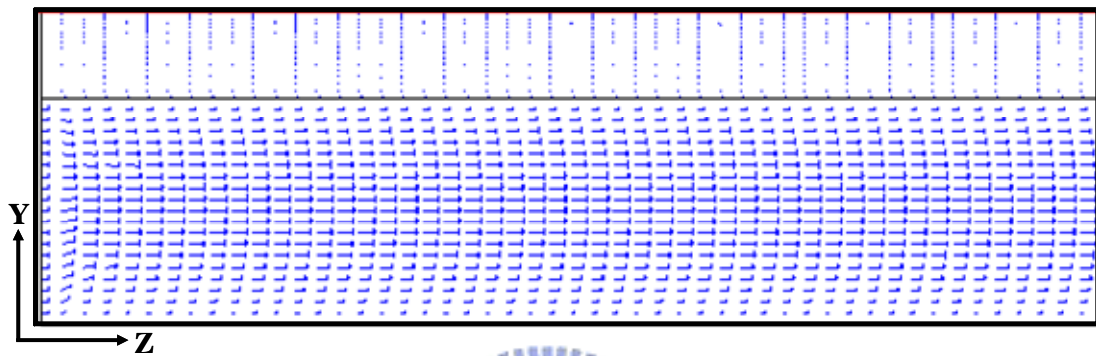


Figure 3.10 Two-phase mixture velocity field in the gas diffusion layer and flow channel of the cathode at the cell voltage of 0.7 V and cathode relative humidity of 80 %.

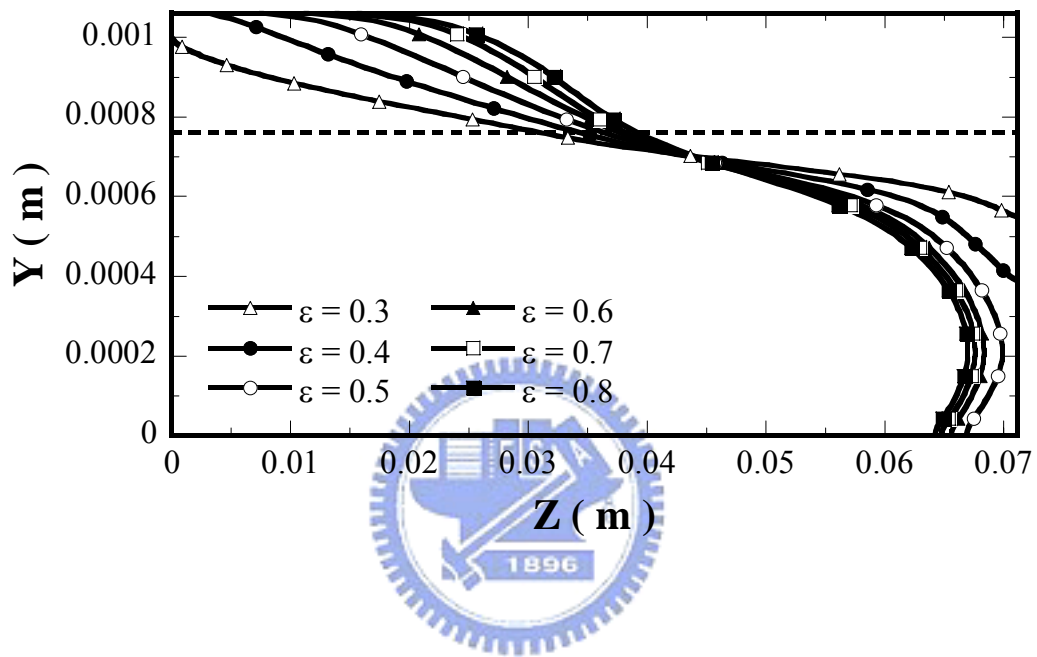


Figure 3.11 Effects of porosity of the gas diffusion layer on the location of the interface where liquid water begins to condense along the conventional flow channel at a cell voltage of 0.7 V and cathode relative humidity of 80 %.

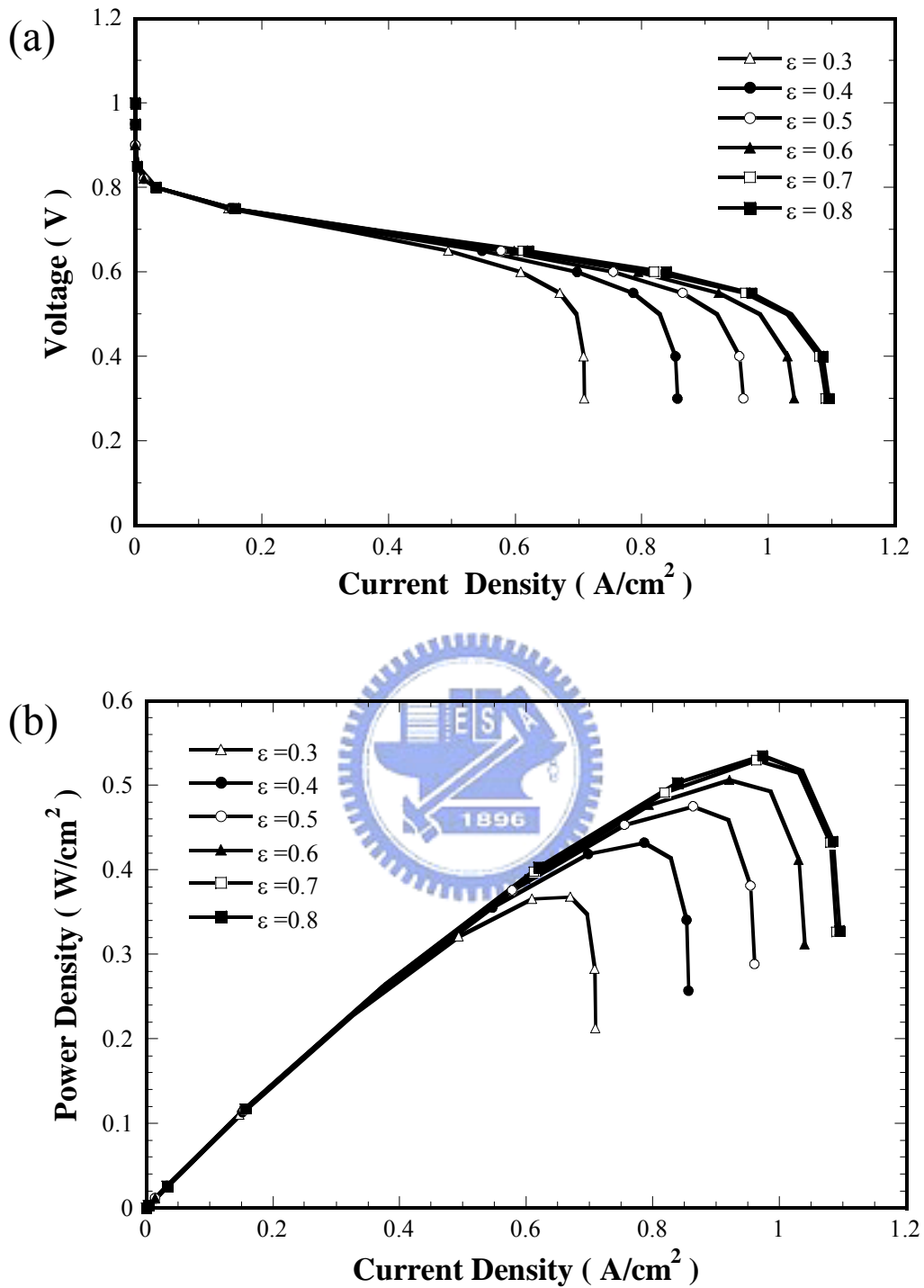


Figure 3.12 Effect of porosity of the gas diffusion layer on cell performance with conventional flow fields at cathode relative humidity of 80 %. (a)  $I$ - $V$  curves and (b)  $I$ - $P$  curves.

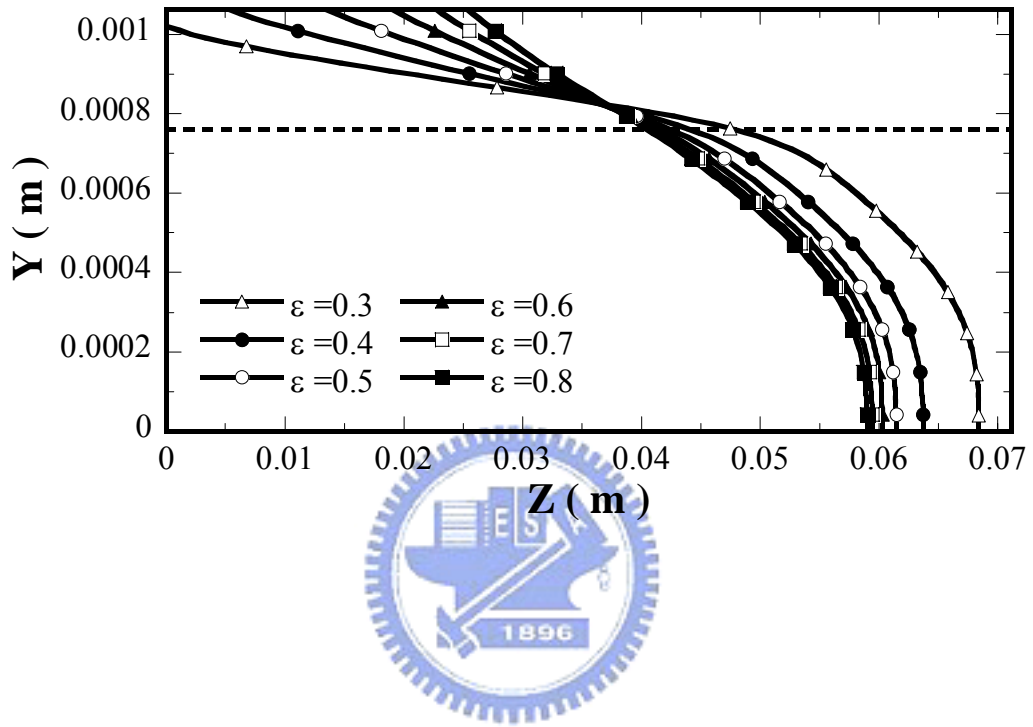


Figure 3.13 Oxygen fraction at various porosities of the gas diffusion layer at an operating voltage of 0.7 V and cathode relative humidity of 80 %.

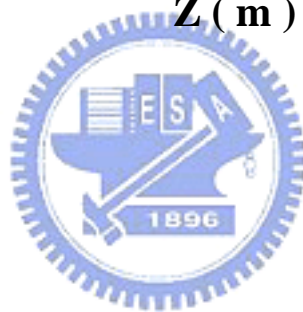
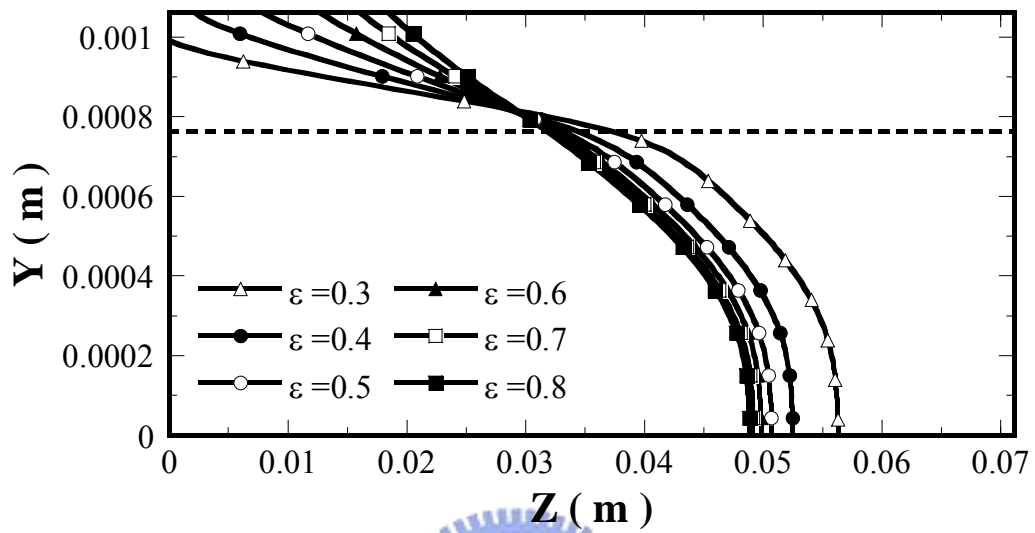


Figure 3.14 Water fraction at various porosities of the gas diffusion layer at an operating voltage of 0.7 V and cathode relative humidity of 80 %.

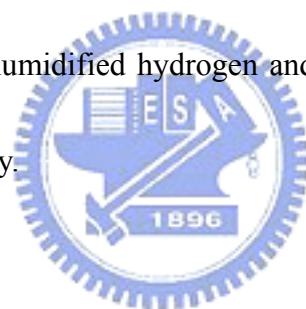
## CHAPTER 4

### EFFECTS OF TEMPERATURE ON THE LOCATION OF THE GAS-LIQUID INTERFACE IN A PEM FUEL CELL

#### 4.1 Introduction

During the operation of a PEM fuel cell, the production of electrical energy is accompanied by the release of thermal energy. The generated heat in a fuel cell includes entropic heat of reactions, the irreversible heat of electrochemical reactions, and Joule heating. It is crucial to keep the cell temperature of the PEM fuel cell within safe levels through proper thermal management to maintain the cell performance properly. This is because a too high cell temperature may lead to membrane dehydration and a too low cell temperature may result in water condensation or even electrodes flooding phenomenon. In order to ensure proper water and thermal managements for the PEM fuel cell, it is essential to predict the water and temperature distributions inside the PEM fuel cell. The formation of liquid water depends on the saturation vapor pressure, which is strongly dependent on the temperature. Therefore, the temperature factor is an inevitable consideration in water management investigations because the phase change of water such as condensation and/or evaporation closely relates to the corresponding saturation pressure.

In this chapter, the non-equilibrium conditions of partial pressure deviation from saturation pressure have been considered. Our quest to delineate the effects of the gas-liquid interface on a PEM fuel cell has involved the following two parts. First, as a preliminary study, the cell temperature and humidification temperature were set as being equal. Second, we considered a scenario whereby cell temperatures were altered at a fixed humidification temperature. For all of the calculations carried out in this study, the fuel flows were co-flows and inlet stoichiometric ratios of 1.5 and 3 were used for the anode and cathode sides based on a reference current density of  $1 \text{ A/cm}^2$ . Furthermore, fully humidified hydrogen and oxygen were fed to the anode and cathode inlets, respectively.



#### ***4.2 Effects of temperatures scheme***

Figure 4.1 shows the polarization curves of the cell at equal cell and humidification temperatures of 323, 333, and 343 K. The results reveal that the cell performance improves as the temperature is increased because a higher temperature results in higher catalytic activity and a higher capacity for water removal by evaporation. Hence, increasing the temperature is helpful in reducing the level of flooding. Moreover, a higher cell temperature increases the membrane conductivity and mass diffusivity, and decreases the mass transport resistance. Figure 4.2 presents



the effect of temperature on the location of the interface at which liquid water begins to condense along the cathode flow channel direction at a cell voltage of 0.7 V. Indeed, the interface is defined as the location where the liquid water begins to condense, and so the saturation value behind this interface is greater than zero and this gives rise to the two-phase flow region. The horizontal dotted line indicates the interface between the flow channel and the gas diffusion layer of the cathode. The results reveal that the gas-liquid interface location moves toward the flow channel inlet region as the temperature is decreased, because the formation of liquid water depends on the saturation pressure, which is strongly dependent on the temperature. Liquid water is more easily and quickly condensed at a lower temperature. Additionally, the formation of liquid water may block pore paths for mass transport through the porous diffusion layer to the cathode catalyst layer, thereby reducing cell performance. An increase in temperature increases the saturation pressure of water vapor, in turn increasing the evaporation capacity of the gas stream. However, although not shown here, a high temperature may result in the membrane drying out.

#### ***4.3 Effects of cell temperatures scheme***

In the second part of this study, the effect of cell temperature was investigated for a fixed inlet gas humidification temperature. As the stoichiometric flow ratio and

the humidification temperature do not change in this phase of simulation, the reactant flow rates were kept constant. Polarization curves at  $T_h = 323\text{ K}$  and  $T_h = 343\text{ K}$  at various cell temperatures are plotted in Fig. 4.3. The curves in Fig. 4.3 (a) reveal that the cell performance improves as the cell temperature is increased from 323 to 333 K, but deteriorates as the temperature is further increased from 333 to 343 K. This result probably follows from the fact that the humidification temperature is less than the cell temperature, and the inlet fuel gases are therefore unsaturated. Therefore, water is almost entirely present in vapor form. Accordingly, the mass fraction of water vapor increases along the channel because of evaporation of liquid water from the cathode catalyst layer. Hence, a high temperature reduces the water content of the membrane, dehydrating it, and reducing its ionic conductivity. Figure 4.3 (b) indicates the positive effect of cell temperature on cell performance. Since the humidification temperature exceeds the cell temperature, liquid water forms when the inlet gases enter the flow channel. Some of the liquid water keeps the membrane moist and improves its ionic conductivity. Accordingly, the cell performance improves as the cell temperature is increased.

Some experimental investigations [46–48] have demonstrated that the best working conditions for the single cell are those under which the humidification temperature slightly exceeds the cell temperature. The objective of this study has been

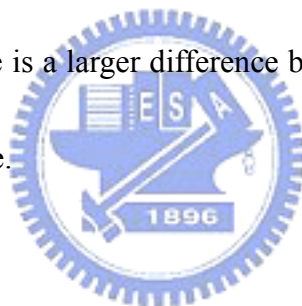
to investigate the impact of the formation of liquid water on cell performance. Therefore, the case in which the humidification temperature exceeds the cell temperature has been considered. Figures 4.4 (a) and (b) show the location of the gas-liquid interface along the flow channel direction at a cell operating voltage of 0.7 V and a humidification temperature of 343 K as the cell temperature is varied. The results reveal that the gas-liquid interface location gradually moves to the gas inlet region as the cell temperature is decreased, which may be ascribed to the following two reasons. (1) Reducing the cell temperature reduces the saturation pressure, increasing the amount of liquid water generated, shifting the gas-liquid interface location closer to the gas channel inlet region. (2) Some of the water produced in the cathode catalyst layer by the electrochemical reaction is evaporated because the cell temperature is higher and, therefore, the gas-liquid interface location moves closer to the cathode catalyst layer. Figure 4.4 (b) shows an enlarged portion of the curves along the channel from 0 to 0.08 cm. In conclusion, reducing the cell temperature can reposition the gas-liquid interface and cause liquid water to appear, which is detrimental to cell performance, since this water may occupy the pores in the porous medium, reducing the amount of fuel gases that can reach the cathode catalyst layer.

#### ***4.4 Three-dimensional species field***

Figure 4.5 displays the liquid water saturation field in the gas flow channel and the gas diffusion layer on the cathode side at various cell temperatures. Each of the figures reveals that liquid water saturation increases along the flow channel direction, because water is generated in the cathode catalyst layer by an electrochemical reaction. Therefore, liquid water may first appear near the interface between the membrane and the cathode catalyst layer close to the channel outlet region. Consequently, the liquid water saturation level in the catalyst layer is higher than that in the gas diffusion layer on the cathode side. Liquid water is transported from the cathode catalyst layer towards the gas diffusion layer only by capillary action; when the liquid water has reached the interface between the flow channel and the gas diffusion layer, it is transported along the channel by the drag force arising from the convective flow of gas.

Figures 4.6 and 4.7 show plots of the distributions of liquid water saturation and temperature in the X-Y section of the cathode gas diffusion layer in the inlet region at a cell voltage of 0.7 V and a humidification temperature of 343 K at various cell temperatures. Figure 4.6 reveals that the liquid water saturation increases under the land and that the amount of liquid water decreases as the cell temperature is increased. In the gas diffusion layer, two transport mechanisms operate — gas-phase diffusion as a result of the concentration gradient from the channel to the land and

liquid water transport by capillary forces from the land to the channel. The liquid water cannot be discharged by the land, so the liquid water saturation on the land is higher than that in the channel. Additionally, the amount of liquid water decreases as the cell temperature is increased because the saturation pressure increases. Figure 4.7 shows that the temperature gradually decreases from the channel to the land. This result has two explanations. (1) Gas-phase diffusion occurs from the channel area to the land; (2) heat produced in the cathode catalyst layer by the electrochemical reaction causes the temperature gradient. Additionally, the degree of temperature variation is greater when there is a larger difference between the cell temperature and the humidification temperature.



#### ***4.5 Temperature field in the membrane***

Figure 4.8 compares the temperature distributions in the membrane from 323 to 343 K. Each of these figures reveals that the temperature distributions in the membrane gradually decline along the flow channel, and that the distribution is symmetric about the  $z$ -center line. Since the inlet gas is fully humidified, the rate of the reaction and the temperature are higher at the inlet. The temperature variation involves irreversible heat, entropic heat, Joule heating, and latent heat. Additionally, the degree of temperature variation in the membrane is greater when there is a larger

difference between the cell temperature and the humidification temperature.

#### **4.6 Summary**

A three-dimensional, non-isothermal, multi-component, and two-phase mathematical model has been developed in the framework of the computational fluid dynamics code. The effects of temperature on the location of the gas-liquid interface along the flow channel direction have been investigated. According to the presented results and the analysis, when the anode and cathode humidification temperatures are equal to or higher than the cell temperature, the gas-liquid interface location moves toward the flow channel inlet region as the temperature is decreased. Since the formation of liquid water may block pore paths for mass transport through the porous diffusion layer to the cathode catalyst layer, cell performance is reduced. An increase in temperature increases the saturation pressure of water, in turn increasing the evaporation capacity of the gas stream. The temperature distributions in the membrane gradually decline along the flow channel direction. The distribution is symmetric about the  $z$ -center line because the cell reaction rate and the temperature are higher at the inlet region. Numerical analysis of the results of this study has also shown that gas-phase fluid diffuses from the channel to the land and that the capillary-driven liquid water is transported in the opposite direction. Additionally, the

degree of temperature variation is greater when there is a large difference between the cell temperature and the humidification temperature.



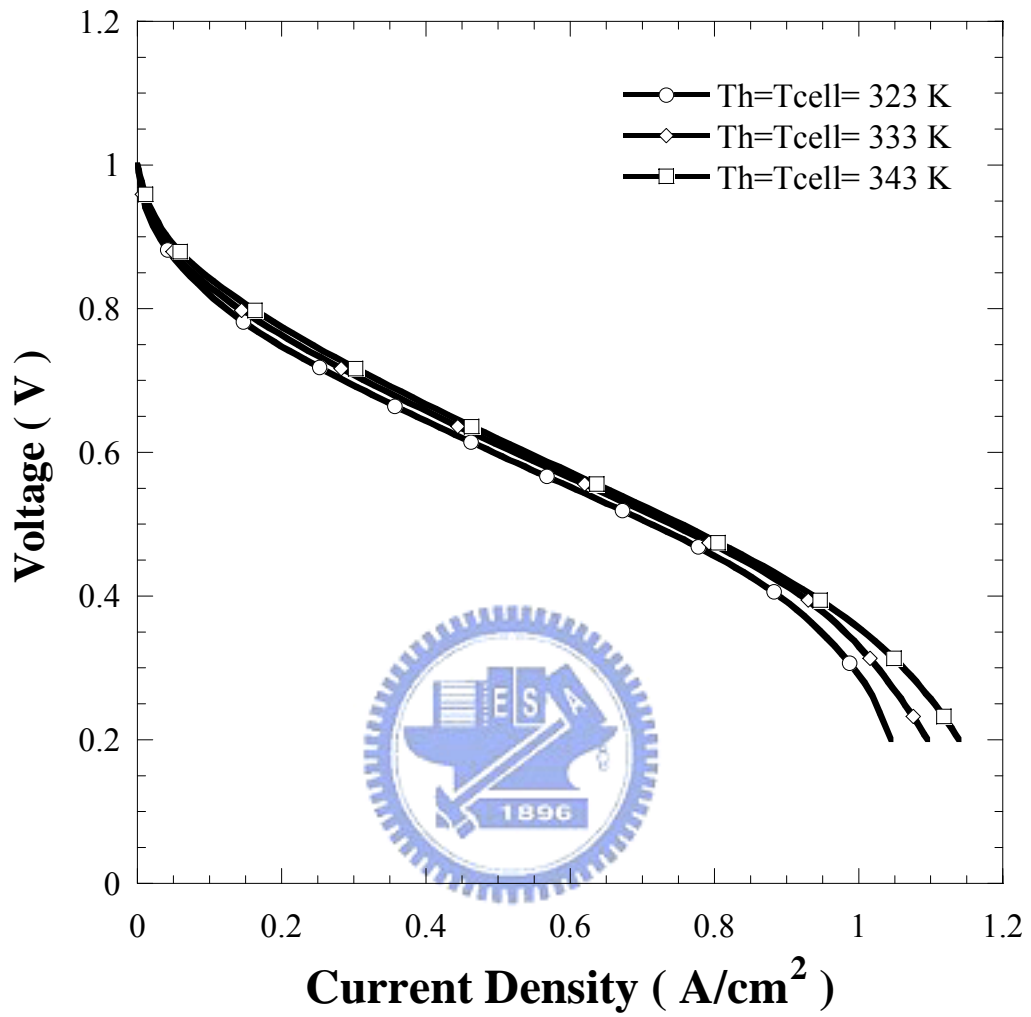


Figure 4.1 Polarization curves at various cell temperatures with equal humidification temperature.



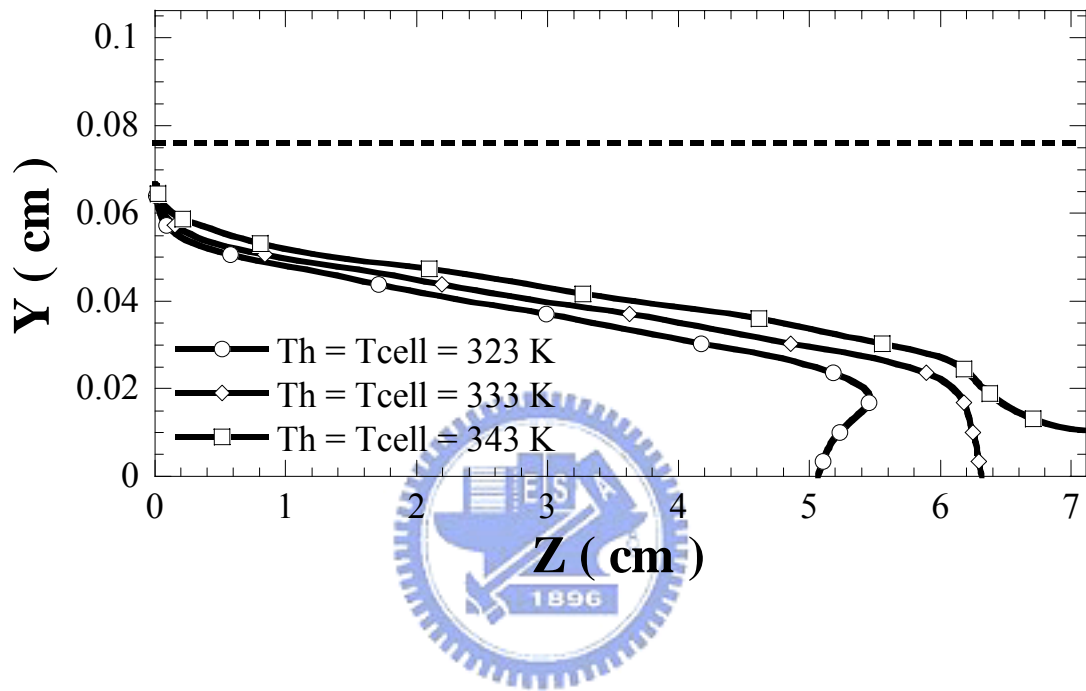


Figure 4.2 Effect of cell temperature on the location of the interface where liquid water begins to condense along the flow channel at a cell operating voltage of 0.7 V.

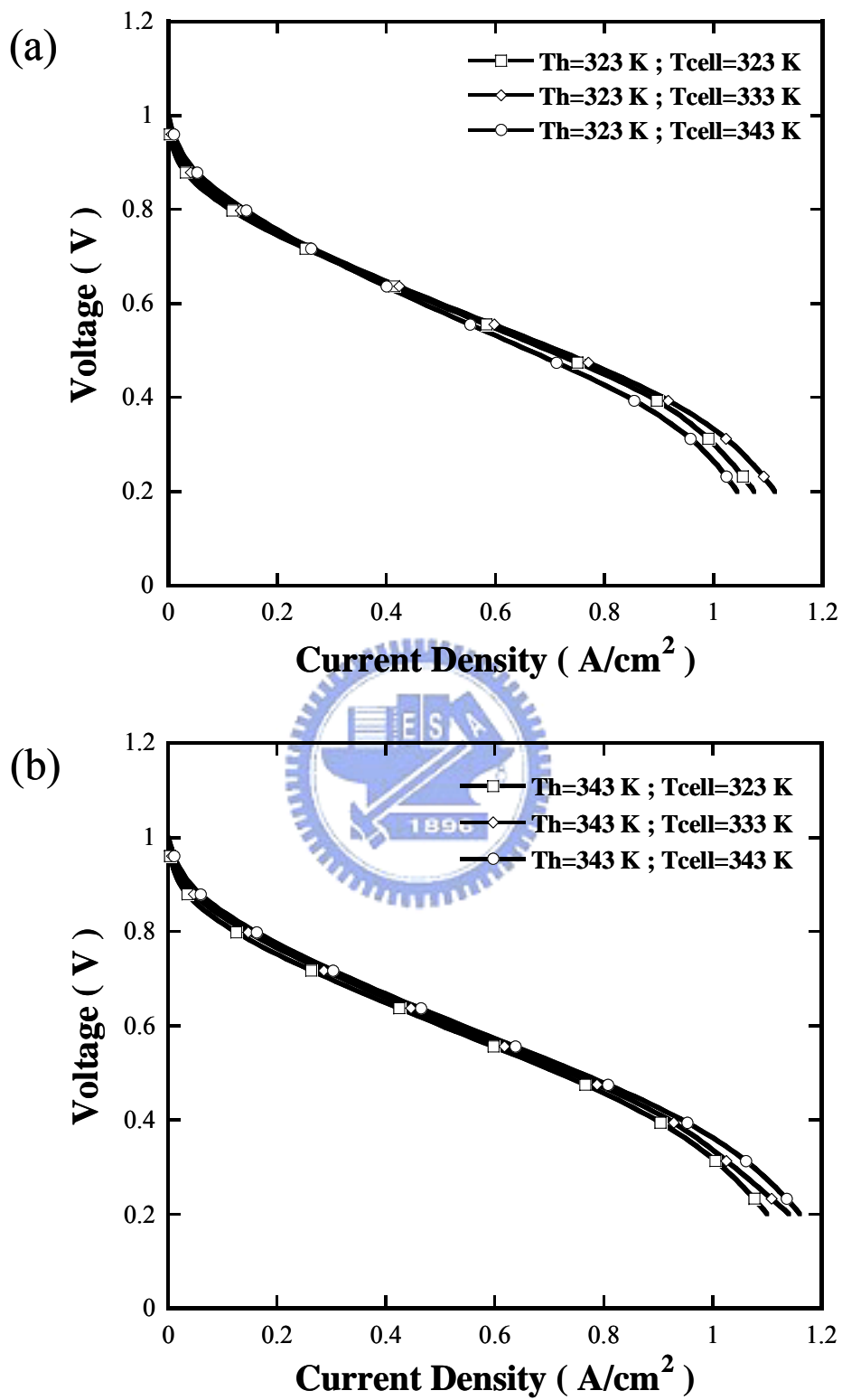


Figure 4.3 Polarization curves for various cell temperatures at (a) Th = 323 K, (b) Th = 343 K.

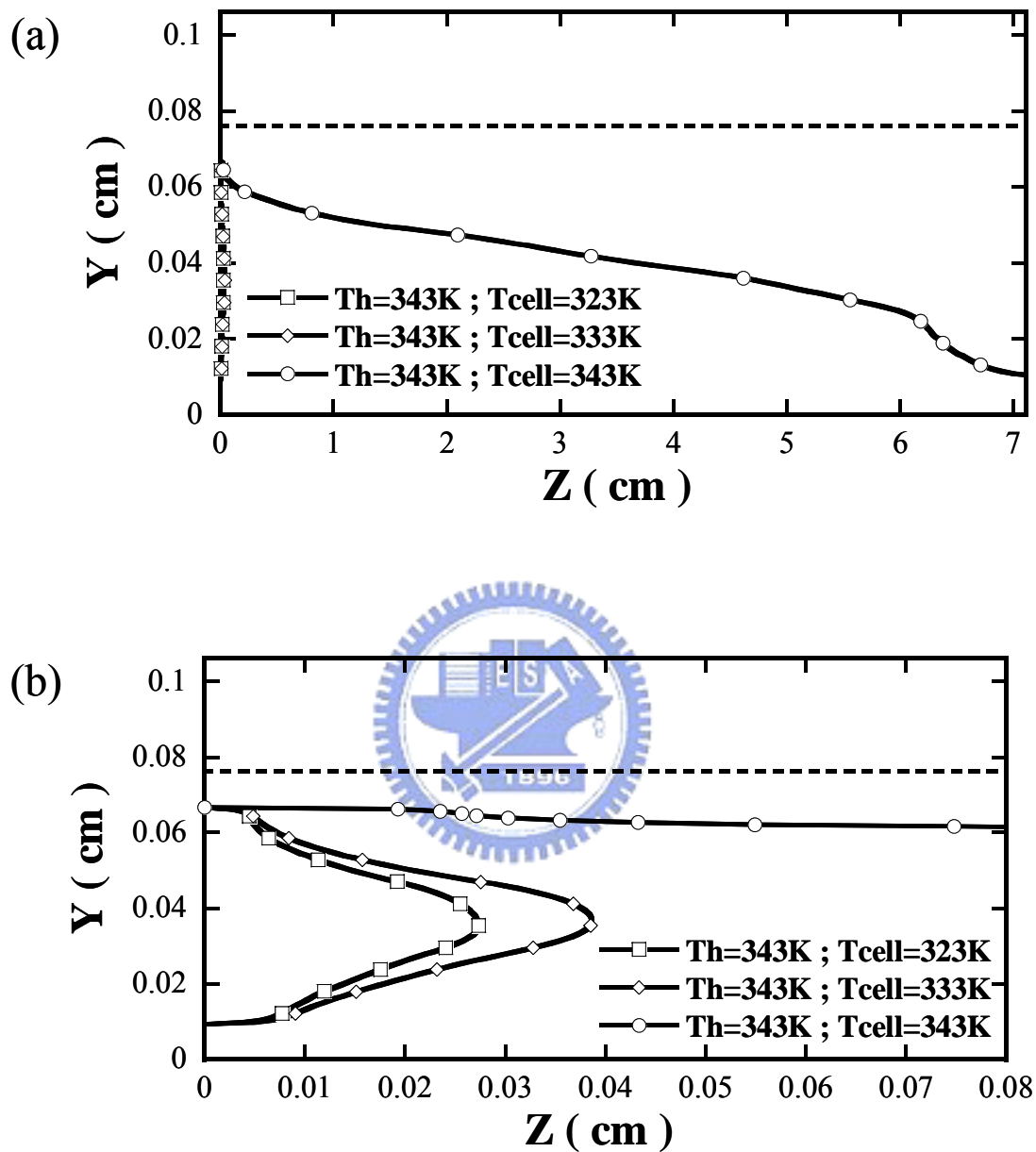


Figure 4.4 Effects of cell temperature on the location of the interface where liquid water begins to condense along the flow channel at a cell operating voltage of 0.7 V and a humidification temperature of 343 K. (a)  $Z = 0$  to 7.112 cm, (b)  $Z = 0$  to 0.08 cm.

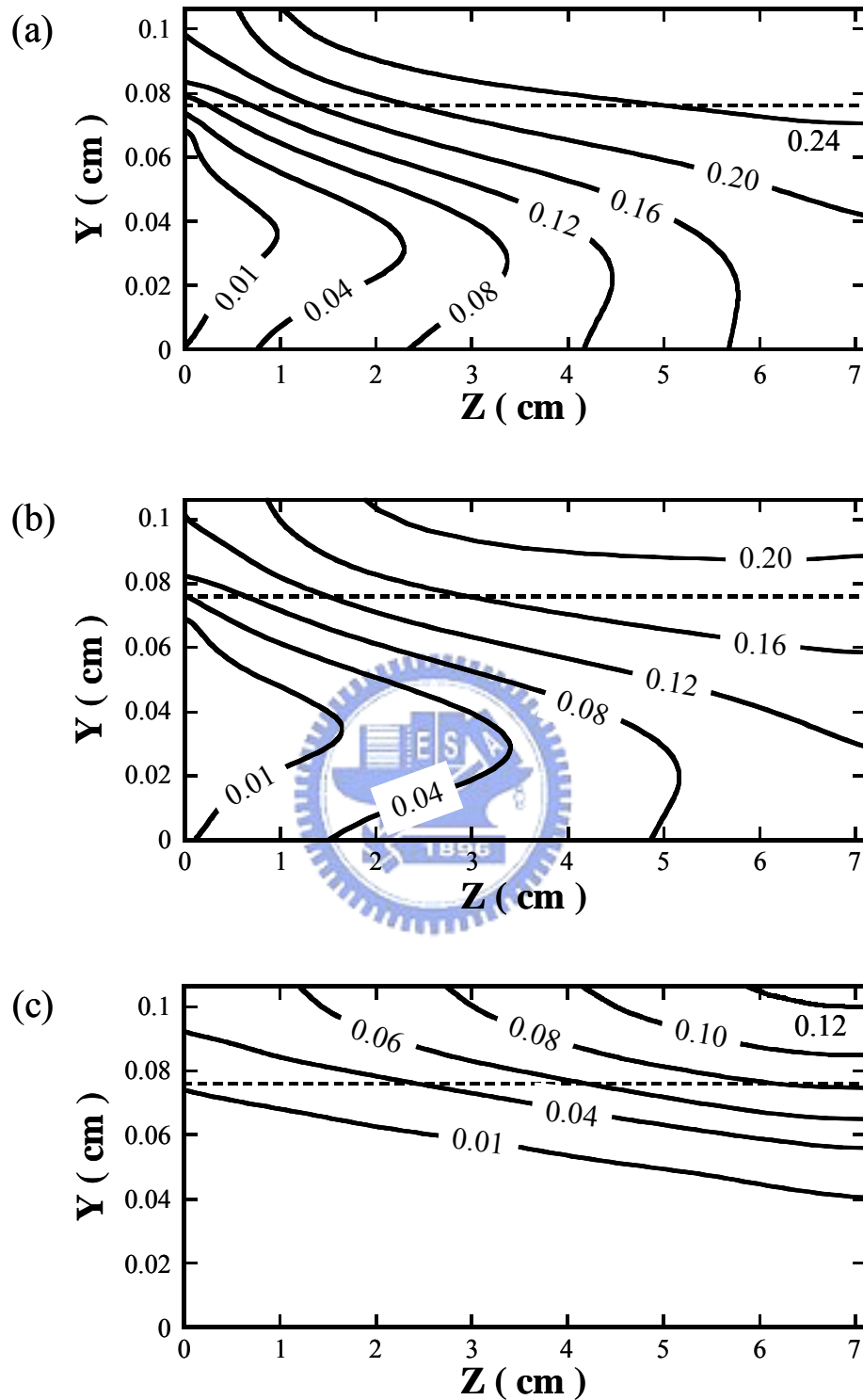


Figure 4.5 Liquid water saturation field in the cathode gas channel and diffusion layer along the flow channel at a cell voltage of 0.7 V and a humidification temperature of 343 K. (a)  $T_{cell} = 323$  K, (b)  $T_{cell} = 333$  K, (c)  $T_{cell} = 343$  K.

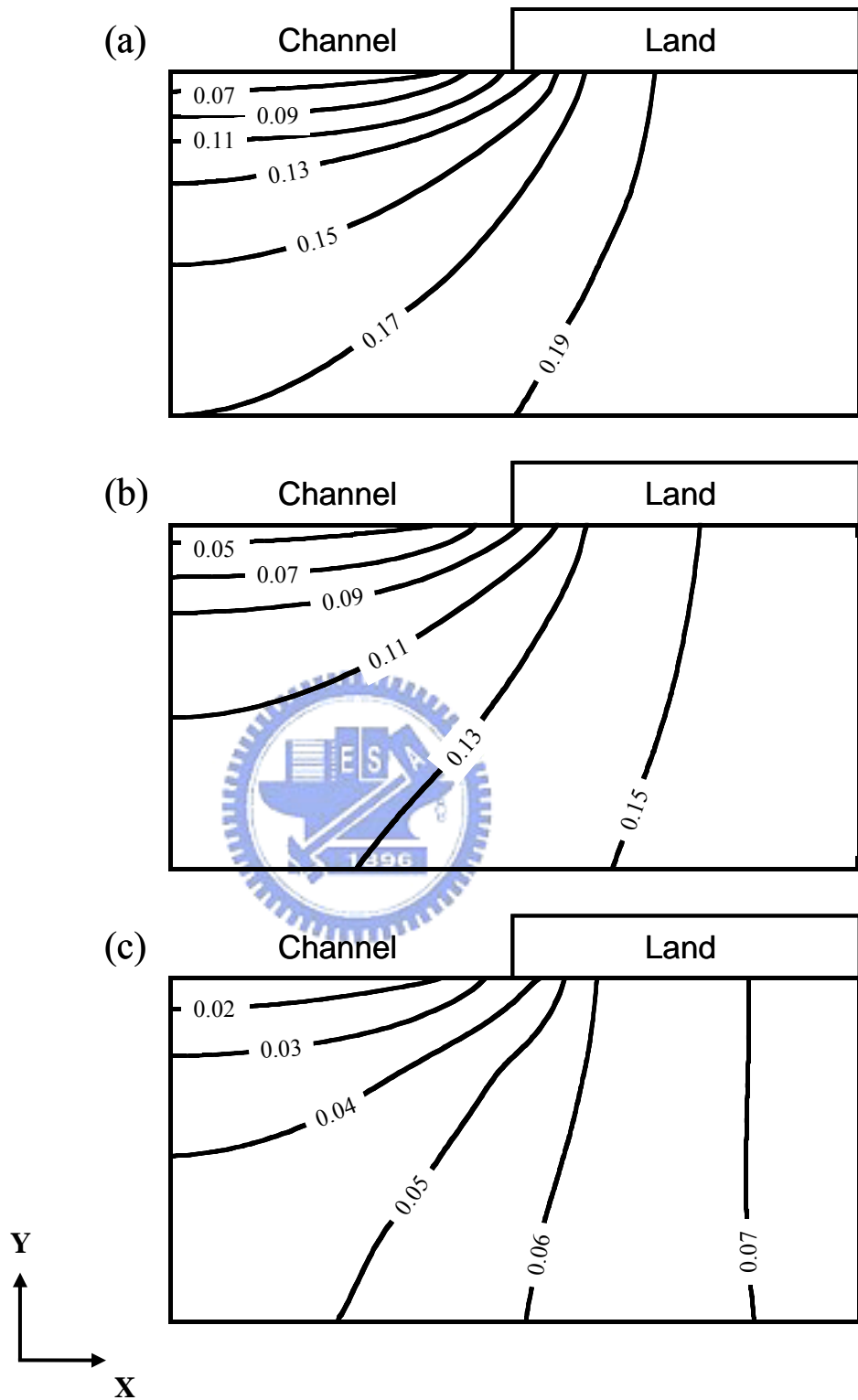


Figure 4.6 Liquid water saturation distributions in a cross-section of the cathode gas diffusion layer in the inlet region at a cell voltage of 0.7 V and a humidification temperature of 343 K. (a)  $T_{cell} = 323\text{ K}$ , (b)  $T_{cell} = 333\text{ K}$ , (c)  $T_{cell} = 343\text{ K}$ .

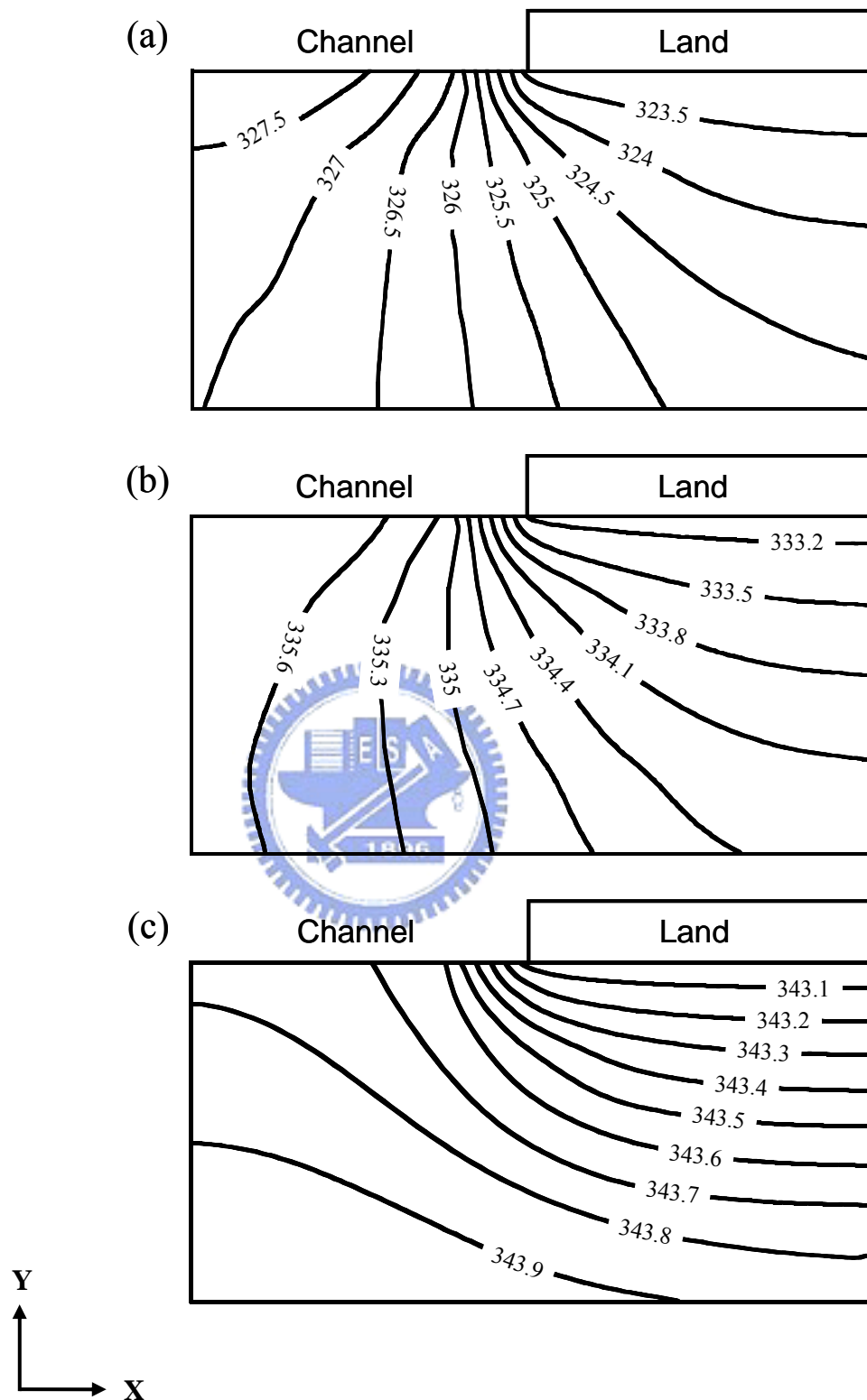


Figure 4.7 Temperature distributions in a cross-section of the cathode gas diffusion layer in the inlet region at a cell voltage of 0.7 V and a humidification temperature of 343 K. (a)  $T_{cell} = 323\text{ K}$ , (b)  $T_{cell} = 333\text{ K}$ , (c)  $T_{cell} = 343\text{ K}$ .

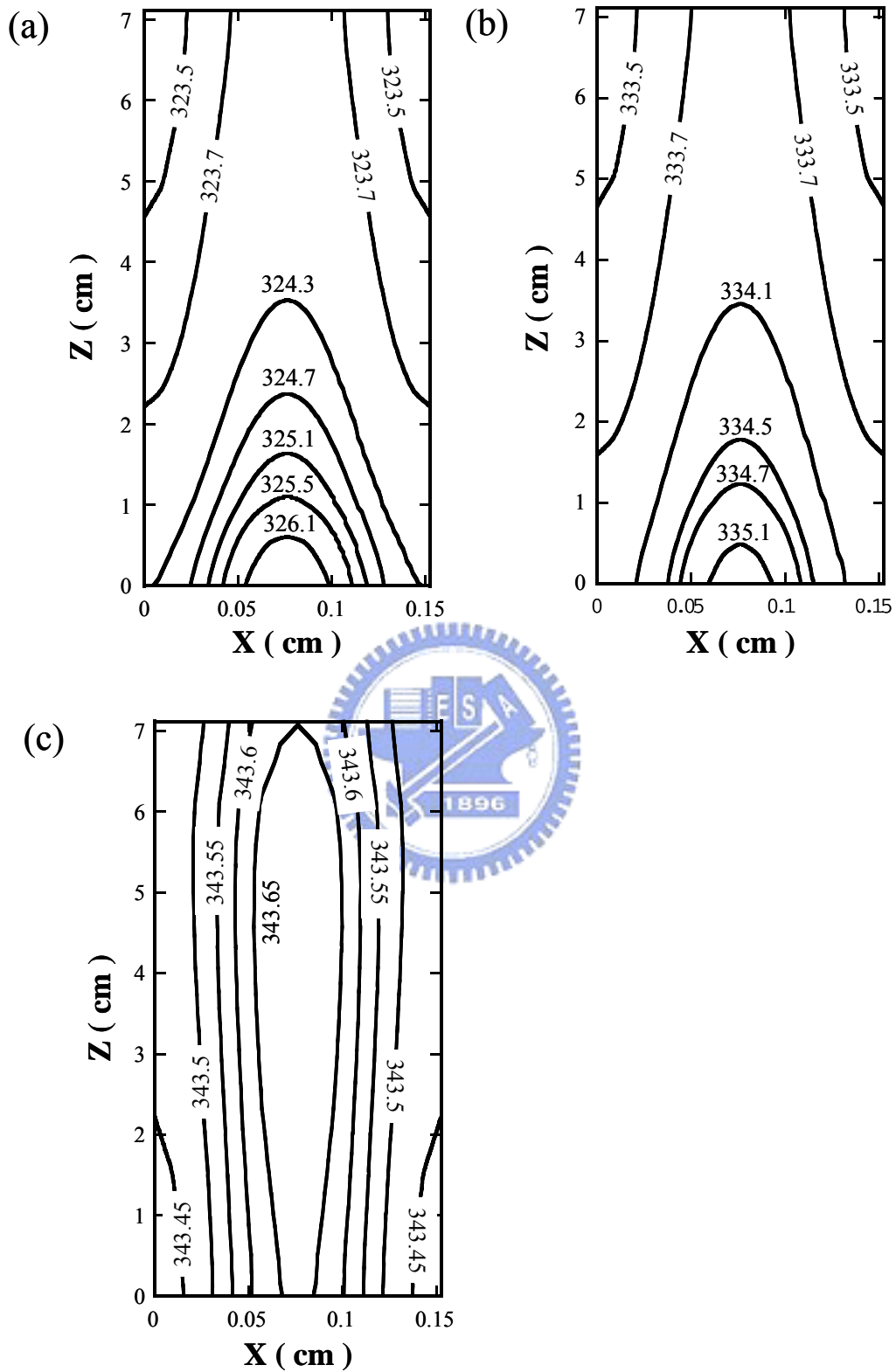


Figure 4.8 Temperature contours in the membrane at a cell voltage of 0.7 V and a humidification temperature of 343 K. (a)  $T_{cell} = 323$  K, (b)  $T_{cell} = 333$  K, (c)  $T_{cell} = 343$  K.

## CHAPTER 5

### CONCLUSIONS AND FUTURE PERSPECTIVES

#### 5.1 *Concluding Remarks*

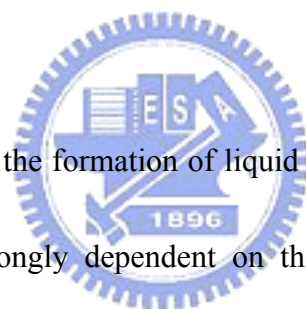
In this dissertation, a single-domain formulation has been developed to comprehensively describe the electrochemical kinetics, current distribution, hydrodynamics, thermal flow, and multi-component transport in a PEM fuel cell. The governing equations considering the mass, momentum, species, charge, and energy conservation with their related boundary conditions are solved using a commercial code based on the SIMPLE algorithm for convection-diffusion problems. A computational fluid dynamics (CFD) technique is successfully adapted to simulate multi-dimensional behaviors of the PEM fuel cell. It is able to predict not only the polarization curves which are consistent with the experimental work of Squadrito *et al.* [44] but also the detailed reactant and product distributions inside the fuel cell.

The scope in this study has included three crucial topics, namely the effects of cathode humidification level, cathode gas diffusion layer porosity and operating temperature on the gas-liquid interface location along the flow channel direction in a PEM fuel cell. The effects of cathode humidification are investigated firstly. It is



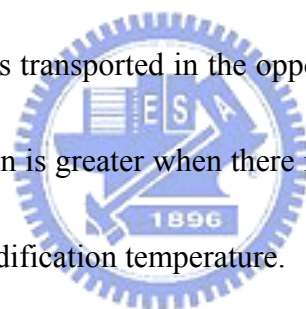
found that the cell performance decreases as the relative humidity of the cathode increases, because the amount of liquid water increases with the relative humidity. Accordingly, the pores in the porous media are obstructed by liquid water at the cathode-side, reducing the amount of reaction gas to the cathode catalyst layer. Therefore, the performance of the cell gradually decreases. The phenomena have also been expounded from the gas-liquid interface location. The gas-liquid interface location moves from the cathode catalyst layer toward the gas diffusion layer and the flow channel as the relative humidity of the cathode increases. Furthermore, when the relative humidity of the cathode reaches 100%, the gas-liquid interface location is close to the gas flow channel inlet region. Hence, the two-phase region appears early to cause the clogging effect of the reactant transport, resulting in the deteriorations of cell performance and power density. Moreover, the cell operating voltage also influences the gas-liquid interface location. Because of the higher cell operating voltage indicates that the lower current density, namely lower electrochemical reaction rate and less water generation rate. Hence, the gas-liquid interface location gradually moves to the gas flow channel inlet region as the operating voltage decreases, because reducing the operating voltage increases the current density and electrochemical reaction rate. The cathode gas diffusion layer porosity also influences the gas-liquid interface location. When the gas diffusion layer porosity decreases, the

gas-liquid interface location appears early in the cathode gas diffusion layer because of the liquid water transport by capillary force is not easy to pass through the gas diffusion layer and spread throughout in it. Hence, the liquid water occupies the pores, causing the limitation of reactant gas diffusion and reducing the cell performance. Nevertheless, if the cathode gas diffusion layer porosity is 0.7, the cell performance and the gas-liquid interface location do not change obviously. The decreased oxygen fraction and the increased water fraction along the flow channel direction are related to the electrochemical reaction of the cathode catalyst layer, as oxygen is consumed and water produced.



Owing to the fact that the formation of liquid water depends on the saturation vapor pressure, which is strongly dependent on the temperature, the temperature factor is an inevitable consideration in water management investigations. Therefore, the developed model is used to investigate the impacts of temperature on the location of the gas-liquid interface along the flow channel direction in a PEM fuel cell. It is found from the result that when the anode and cathode humidification temperatures are equal to or higher than the cell temperature, the gas-liquid interface location moves toward the flow channel inlet region as the temperature is decreased. Because of a lower temperature results in lower catalytic activity and a lower capacity for water removal by evaporation to cause flooding phenomena. Hence, there is an earlier

formation of the two-phase region to cause the cell performance decreased. The temperature in the membrane gradually decline along the flow channel direction because the reactant rate and the temperature are higher at the inlet region. Furthermore, the distribution is symmetric about the  $z$ -center line because of the oxygen is consumed and water is produced in the channel region higher than the ribs region. Moreover, the distributions of liquid water saturation and temperature in the X-Y section of the cathode gas diffusion layer in the inlet region are investigated. The results show that gas-phase fluid diffuses from the channel to the land and that the capillary-driven liquid water is transported in the opposite direction. Additionally, the degree of temperature variation is greater when there is a large difference between the cell temperature and the humidification temperature.



## ***5.2 Future works***

It has been demonstrated that proper water and heat management is crucial for achieving high power density performance at high energy efficiency for proton exchange membrane fuel cells. In particular, the two-phase flow phenomena appear in the cell domain. Because of the formation of liquid water depends on the saturation pressure, which is strongly dependent on the temperature, the complex mechanism of the two-phase flow in association with heat transport must be considered in the

modeling study of PEM fuel cell. The investigations and findings in previous chapters offer an essential knowledge base for the subsequent study. Numerical simulations show that liquid water is mainly produced in the gas diffusion layer in two regions; one is near the current-collector land owing to the low temperature and another one is inside the gas diffusion layer but still away from the cathode catalyst layer. Furthermore, from the calculation result, it is shown that the gas-liquid interface location affects the cell performance. Therefore, if the location of the gas-liquid interface could be shifted toward channel downstream, the amount of fuel gas that enters the gas diffusion layer and the cell performance would be increased accordingly. Hence, this result suggests a new role of the micro-porous layer that is at least at the inlet region of the cell, it serves to prevent liquid water from entering the catalyst layer and thus alleviates severe liquid water flooding in the region. The effect and transport characteristics of this new component on the water and thermal management of PEM fuel cells needs to be further verified and considered in the future modeling efforts.

## REFERENCE

- [1]. J. Larminie and A. Dicks: Fuel Cell Systems-Explained, Wiley, 2003.
- [2]. D.M. Bernardi and M.W. Verbrugge, "Mathematical Model of a Gas Diffusion Electrode Bonded to a Polymer Electrolyte," AIChE J. vol.37, pp. 1151-1163, 1991.
- [3]. D.M. Bernardi and M.W. Verbrugge, "A Mathematical Model of the Solid-Polymer-Electrolyte Fuel Cell," J. Electrochem. Soc., vol. 139, no. 9, pp. 2477-2491, 1992.
- [4]. T.E. Springer, T.A. Zawodzinski, and S. Gottesfeld, "Polymer Electrolyte Fuel Cell Model," J. Electrochem. Soc., vol. 138, no.8, pp. 2334-2342, 1991.
- [5]. T.E. Springer, M.S. Wilson, and T.A. Zawodzinski, "Modeling and Experimental Diagnostics in Polymer Electrolyte Fuel Cells," J. Electrochem. Soc. vol. 140, no.12, pp. 3513–3526, 1993.
- [6]. T.F. Fuller and J. Neuman, "Water and Thermal Management in Solid-Polymer-Electrolyte Fuel Cells," J. Electrochem. Soc., vol. 140, no. 5, pp. 1218-1225, 1993.
- [7]. T.V. Nguyen and R.E. White, "A Water and Heat Management Model for Proton-Exchange-Membrane Fuel Cells," J. Electrochem. Soc., vol. 140, no. 8,

pp. 2178-2196, 1993.

- [8]. J.S. Yi and T.V. Nguyen, "An along-the-channel Model for Proton Exchange Membrane Fuel Cells," *J. Electrochem. Soc.*, vol. 145, no. 4, pp. 1149-1159, 1998.
- [9]. V. Gurau, H.T. Liu, and S. Kakac, "Two-Dimensional Model for Proton Exchange Membrane Fuel Cells," *AIChE J.*, vol. 44, no. 11, pp. 2410-2422, 1998.
- [10]. J.S. Yi and T.V. Nguyen, "Multicomponent Transport in Porous Electrodes of Proton Exchange Membrane Fuel Cells Using the Interdigitated Gas Distributors," *J. Electrochem. Soc.*, vol. 146, no. 1, pp. 38-45, 1999.
- [11]. Z.H. Wang, C.Y. Wang, and K.S. Chen, "Two-Phase Flow and Transport in the Air Cathode of Proton Exchange Membrane Fuel Cells," *J. Power Sources*, vol. 94, pp. 40-50, 2001.
- [12]. C.Y. Wang and P. Cheng, "A Multiphase Mixture Model for Multiphase, Multicomponent Transport in Capillary Porous Media I. Model Development," *Int. J. Heat Mass Transfer*, vol. 39, no. 17, pp. 3607-3618, 1996.
- [13]. L. You and H.T. Liu, "A Two-Phase Flow and Transport Model for the Cathode of PEM Fuel Cell," *Int. J. Heat Mass Transfer*, vol. 45, pp. 2277-2287, 2002.

- [14]. S. Mazumder and J.S. Cole, "Rigorous 3-D Mathematical Modeling of PEM Fuel Cells I. Model Prediction without Liquid Water Transport," J. Electrochem. Soc., vol. 150, no. 11, pp. A1503-A1509, 2003.
- [15]. S. Mazumder and J.S. Cole, "Rigorous 3-D Mathematical Modeling of PEM Fuel Cells II. Model Prediction with Liquid Water Transport," J. Electrochem. Soc., vol. 150, no. 11, pp. A1510-A1517, 2003.
- [16]. U. Pasaogullari and C.Y. Wang, "Two-Phase Modeling and Flooding Prediction of Polymer Electrolyte Fuel Cell," J. Electrochem. Soc., vol. 152, no. 2, pp. A380-A390, 2005.
- [17]. W. He, J.S. Yi, and T.V. Nguyen, "Two-Phase Flow Model of the Cathode PEM Fuel Cell Using Interdigitated Flow Fields," AIChE J., vol. 46, no. 10, pp. 2053-2064, 2000.
- [18]. D. Natarajan and T.V. Nguyen, "A Two-Dimensional Two-Phase Multicomponent Transient Model for the Cathode of a Proton Exchange Membrane Fuel Cell Using Conventional Gas Distributors," J. Electrochem. Soc., vol. 148, pp. A1324-A1335, 2001.
- [19]. H. Meng and C.Y. Wang, "Modeling of Two-Phase Flow and Flooding Dynamics in Polymer Electrolyte Fuel Cell," J. Electrochem. Soc., vol. 152, no. 9, pp. A1733-A1741, 2005.

- [20]. F.Y. Zhang, X.G. Yang, and C.Y. Wang, "Liquid Water Removal from a Polymer Electrolyte Fuel Cell," *J. Electrochem. Soc.*, vol. 153, no. 2, pp. A225-A232, 2006.
- [21]. A. Rowe and X. Li, "Mathematical Modeling of Proton Exchange Membrane Fuel Cells," *J. Power Sources*, vol. 102, pp. 82-96, 2001.
- [22]. J.J. Baschuk and X. Li, "Modeling of Polymer Electrolyte Membrane Fuel Cells with Variable Degree of Water Flooding," *J. Power Sources*, vol. 86, pp. 181-196, 2000.
- [23]. N. Djilali and D. Lu, "Influence of Heat Transfer on Gas and Water Transport in Fuel Cells," *Int. J. Therm. Sci.*, vol. 41, pp. 29-40, 2002.
- [24]. S. Sempalee and S. Dutta, "Numerical Prediction of Temperature Distribution in PEM Fuel Cells," *Numerical Heat Transfer, Part A*, vol. 38, pp. 111-128, 2000.
- [25]. D. Natarajan and T.V. Nguyen, "Three-Dimensional Effects of Liquid Water Flooding in the Cathode of a PEM Fuel Cell," *J. Power Sources*, vol. 115, pp. 66-80, 2003.
- [26]. X.G. Yang, F.Y. Zhang, A.L. Lubawy, C.Y. Wang, "Visualization of Liquid Water Transport in a PEFC," *Electrochem. Solid-State Lett.*, vol. 7, no. 11, pp. A408-A411, 2004.



- [27]. X. Liu, H. Guo, and C. Ma, "Water Flooding and Two-Phase Flow in Cathode Channels of Proton Exchange Membrane Fuel Cells," *J. Power Sources*, vol. 156, pp. 267-280, 2006.
- [28]. H. Ju, H. Meng, and C.Y. Wang, "A Single-Phase, Non-Isothermal Model for PEM Fuel Cells," *Int. J. Heat Mass Trans.*, vol. 48, pp. 1303-1315, 2005.
- [29]. Y. Wang and C.Y. Wang, "A Nonisothermal, Two-Phase Model for Polymer Electrolyte Fuel Cells," *J. Electrochem. Soc.*, vol. 153, no. 6, pp. A1193-A1200, 2006.
- [30]. S. Dutta, S. Shimpalee, and J.W. Van Zee, "Three-Dimensional Numerical Simulation of Straight Channel PEM Fuel Cells," *J. Appl. Electrochem.*, vol. 30, pp. 135-146, 2000.
- [31]. S. Dutta, S. Shimpalee, and J.W. Van Zee, " Numerical Prediction of Mass-Exchange between Cathode and Anode Channels in a PEM Fuel Cell," *Int. J. Heat and Mass Trans.*, vol. 44, pp. 2029-2042, 2001.
- [32]. W.M. Yan, C.Y. Soong, F. Chen, and H.S. Chu, "Effects of Flow Distributor Geometry and Diffusion Layer Porosity on Reactant Gas Transport and Performance of Proton Exchange Membrane Fuel Cells," *J. Power Sources*, vol. 125, pp. 27-39, 2004.
- [33]. H.C. Liu, W.M. Yan, C.Y. Soong, and F. Chen, "Effects of Baffle-Blocked

Flow Channel on Reactant Transport and Cell Performance of a Proton Exchange Membrane Fuel Cell,” J. Power Sources, vol. 142, pp. 125-133, 2005.

[34]. C.Y. Soong, W.M. Yan, C.Y. Tzeng, H.C. Liu, F. Chen, and H.S. Chu, “Analysis of Reactant Gas Transport in a PEM Fuel Cell with Partially Blocked Fuel Flow Channels,” J. Power Sources, vol. 143, pp. 36-47, 2005.

[35]. T. Berning, D.M. Lu, and N. Djilali, “Three-Dimensional Computational Analysis of Transport Phenomena in a PEM Fuel Cell,” J. Power Source, vol. 106, pp. 284-294, 2002.

[36]. T. Berning and N. Djilali, “Three-Dimensional Computational Analysis of Transport Phenomena in a PEM Fuel Cell – A Parametric Study,” J. Power Source, vol. 124, pp. 440-452, 2003.

[37]. S. Um and C.Y. Wang, “Three-Dimensional Analysis of Transport and Electrochemical Reactions in Polymer Electrolyte Fuel Cells,” J. Power Sources, vol. 125, pp. 40-51, 2004.

[38]. M.S. Chiang and H.S. Chu, “Effect of Temperature and Humidification Levels on the Performance of a Proton Exchange Membrane Fuel Cell,” IMechE Part A, J. Power and Energy, vol. 220, pp. 42-53, 2006.

[39]. M.S. Chiang and H.S. Chu, “Numerical Investigation of Transport Component

Design Effect on a Proton Exchange Membrane Fuel Cell,” *J. Power Sources*, vol. 160, pp. 340-352, 2006.

- [40]. C.Y. Wang and C. Beckermann, “A two-phase mixture model of liquid-gas flow and heat transfer in capillary porous media – I. formulation,” *Int. J. Heat Mass Trans.*, vol. 36, pp. 2747-2758, 1993.
- [41]. U. Pasaogullari and C.Y. Wang, “Liquid Water Transport in Gas Diffusion Layer of Polymer Electrolyte Fuel Cells,” *J. Electrochem. Soc.*, vol. 151, no. 3, pp. A399-A406, 2004.
- [42]. U. Pasaogullari and C.Y. Wang, “Two-Phase Transport and the Role of Micro-Porous Layer in Polymer Electrolyte Fuel Cells,” *Electrochim. Acta.*, vol. 49, pp. 4359-4369, 2004.
- [43]. CFD-ACE(U)™ User Manual, CFD Research Corp., Huntsville, AL, 2004.
- [44]. G. Squadrito, G. Maggio, E. Passalacqua, F. Lufrano, and A. Patti, “An Empirical Equation for Polymer Electrolyte Fuel Cell (PEFC) Behaviour,” *J. Appl. Electrochem.*, vol. 29, pp. 1449-1455, 1999.
- [45]. S. Um, C.Y. Wang, and K.S. Chen, “Computational Fluid Dynamics Modeling of Proton Exchange Membrane Fuel Cells,” *J. Electrochem. Soc.*, vol. 147, no. 12, pp. 4485-4493, 2000.
- [46]. L. R. Jordan, A. K. Shukla, T. Behrsing, N. R. Avery, B. C. Muddle, and M.

Forsyth, “Diffusion layer parameters influencing optimal fuel cell performance,” *J. Power Sources*, vol. 86, pp. 250-254, 2000.

[47]. T. J. P. Freire and E. R. Gonzalez, “Effect of membrane characteristics and humidification conditions on the impedance response of polymer electrolyte fuel cells,” *J. Electroanal. Chem.*, vol. 503, pp. 57-68, 2001.

[48]. M. G. Santarelli and M. F. Torchio, “Experimental analysis of the effects of the operating variables on the performance of a single PEMFC,” *Energy Conversion and Management*, vol. 48, pp. 40-51, 2007.



## List of Publications

1. Chun-I Lee and H. S. Chu, “Thermal Radiative Properties for the Ferroelectric Thin Films,” *J. Chinese Society of Mechanical Engineers*, 2003, 977-983.
2. Chun-I Lee and H. S. Chu, “Effects of cathode humidification on the gas-liquid interface location in a PEM fuel cell,” *J. Power Sources*, 2006, 161, 949-956.
3. Chun-I Lee and H. S. Chu, “Effects of Temperature on the Location of the Gas-Liquid Interface in a PEM Fuel Cell,” *J. Power Sources*, 2007, (Published).

